THE EFFECT OF SEPARAN AP-30 ON THE PERFORMANCE OF A 10mm HYDROCYCLONE

Thesis for the Degree of M. S.

MICHIGAN STATE UNIVERSITY

GLEN EUGENE THOMAS

1982

ABSTRACT

THE EFFECT OF SEPARAN AP-30
ON THE PERFORMANCE OF A 10mm
HYDROCYCLONE

By

Glen Eugene Thomas

Present understanding of secondary flow structures within hydrocyclones is insufficient to accurately predict the critical design parameters necessary in many hydrocyclone applications. In this study, an attempt to alter these flow patterns was made by adding small amounts of a high molecular weight polymer to the feed stream of a 10mm hydrocyclone. The resulting effects on the capacity and split ratio were measured. Also, the separation efficiency for kaolinite clay particles ($\sim$1 micron in size) was examined for different polymer-clay-water suspensions having identical concentrations. The results showed that the polymer significantly decreased the underflow stream and either increased or decreased the separation efficiency depending on the solution mixing strategy.

THE EFFECT OF SEPARAN AP-30 ON THE PERFORMANCE OF A 10mm HYDROCYCLONE

By

Glen Eugene Thomas

A THESIS

Submitted to
Michigan State University
in partial fulfillment of the requirements
for the degree of

MASTER OF SCIENCE

Department of Chemical Engineering

1982

To my parents

-and-

To my wife, Barbara

ACKNOWLEDGMENTS

The author gratefully acknowledges the guidance and editorial assistance of Dr. Charles Petty.

Funds for this research were provided by the National Science Foundation grant no. 71-1642 and by the Division of Engineering Research, Michigan State University. This assistance is gratefully appreciated.

Special appreciation is also expressed to my wife, Barbara, for her encouragement and help in the completion of this thesis.

TABLE OF CONTENTS

LIST OF TABLES

LIST OF FIGURES

LIST OF NOTATIONS

c	=	concentration of the polymer or clay
D	=	the diameter of the capillary tube used for friction factor measurements in Appendix A
D_C	=	the diameter of the hydrocyclone
D_F	=	the diameter of the feed (inlet) orifice in the hydrocyclone
D_O	=	the diameter of the overflow (vortex) orifice in a hydrocyclone
D_u	=	the diameter of the underflow (apex) orifice in the hydrocyclone
E	=	centrifugal efficiency as defined in Equation 2.1
f	=	Fanning friction factor used in Appendix A as defined by Equation A.7
g	=	the acceleration due to gravity used in Appendix A
G_O	=	the pressure loss coefficient as defined by Equation 5.3
G_u	=	the pressure loss coefficient as defined by Equation 5.3 but based on the underflow stream
ΔH	=	the height differential for a manometer used in Appendix A
ΔH_C	=	the height differential for a $cc\ell_4$ manometer used in Appendix A
ΔH_M	=	the height differential for a mercury manometer used in Appendix A
K	=	a proportionality constant defined by Equation 2.1; also Equation A.2 in Appendix A
K'	=	a proportionality constant related to K

L	=	the length of the hydrocyclone; also the distance between the pressure taps in Appendix A
N	=	a dimensionless group defined by Equation 5.4 based on Re_F and hydrocyclone dimensions
ΔP	=	the difference between the feed P_F and overflow P_o pressures on the hydrocyclone; also the difference in pressure between the two pressure taps on the capillary tube in Appendix A
P_F	=	the feed pressure on the hydrocyclone
P_o	=	the overflow pressure on the hydrocyclone
P_u	=	the underflow pressure on the hydrocyclone
Q	=	the volumetric flow rate through the capillary tube in Appendix A
Q_F	=	the volumetric flow rate into the feed of a hydrocyclone
Q_o	=	the volumetric flow rate exiting the overflow of a hydrocyclone
Q_u	=	the volumetric flow rate exiting the underflow of a hydrocyclone
R	=	the radius of the capillary tube in Appendix A
Re	=	the Reynolds number for the capillary tube in Appendix A
Re_F	=	the Reynolds number for the feed (inlet) conditions
U_b	=	the bulk average velocity of the fluid inside the capillary tube in Appendix A
U_F	=	the bulk average velocity of the fluid entering the hydrocyclone
W	=	mass flow rate of fluid in the capillary tube in Appendix A
W_F	=	the mass flow rate entering the hydrocyclone
W_o	=	the mass flow rate exiting the overflow of the hydrocyclone

W_u = the mass flow rate exiting the underflow of the hydrocyclone

W_o^*, W_u^*, W_s^* = hypothetical streams used to define E (see Figure 2.2)

X = exponent used in Equation 2.1

X_F = mass fraction of solids in feed stream of a hydrocyclone

X_o = mass fraction of solids in the underflow stream of a hydrocyclone

X_u = mass fraction of solids in the underflow stream of a hydrocyclone

ρ = density of water

$\rho CC\ell_4$ = density of carbon tetrachloride

ρ_M = density of mercury

ρ_s = density of solids

τ_w = shear stress at the wall used in Appendix A to define f

μ = viscosity; also microns when discussing particle diameters

CHAPTER 1

INTRODUCTION

A high molecular weight polymer is added to the feed stream of a hydrocyclone in an attempt to alter internal flow structures and to develop some additional understanding of those flow patterns which most directly affect the separation efficiency. This research extends the work of Wallace [1980] and of Dabir, et al. [1980] by examining the performance of hydrocyclones for 0.2 wt. % suspensions, which is an order of magnitude smaller than previously investigated. This avoids some of the experimental difficulties encountered earlier.

Preliminary results on the effect of a small amount of Separan AP-30 on the separation of kaolinite clays in a 10mm hydrocyclone investigated by Wallace and Dabir in our laboratory showed that for a given pressure drop across the hydrocyclone, the total flow rate is reduced by the presence of the polymer. Presumably, the polymer offers a large resistance to helical flow, similar to the vortex inhibition phenomenon reported by Chiou and Gordon [1976]. A slight increase in the split between the overflow and underflow rates with the addition of polymer was also noticed.

Two mixing strategies for the polymer-clay-water suspensions were examined which showed significantly different separation

behavior. One strategy "pre-stretched" the polymer before the addition of clay by cycling it through a small capillary tube whereas the other strategy omitted this "pre-stretching" step and added a concentrated polymer solution to a dilute clay suspension. An initial increase in the centrifugal efficiency (E) of 63% occurred for the "pre-stretched" strategy. However, the other formulation, although identical in polymer and clay concentration, showed an initial decrease of 77% in E. After about an hour of operation, the centrifugal efficiency of these two suspensions stabilized above and below the no polymer case.

The objective of this research is to examine more carefully the two paradoxical mixing strategies reported earlier by Wallace and Dabir. The effects that these mixing strategies have on the capacity and split ratio are summarized in Section 5.2. Section 5.3 shows the effects of the various mixing strategies on the centrifugal efficiency of the hydrocyclone. Also, the apparent viscosities of the suspensions used in this investigation, as well as their drag reducing characteristics for fully developed turbulent pipe flow, were measured and reported in Appendix A.

CHAPTER 2

BACKGROUND

2.1 The Hydrocyclone

The liquid cyclone or hydrocyclone is a processing device that uses pressure to create rotational motion in a body of fluid thus generating a centrifugal force that separates one material from another. Basically, the hydrocyclone separator is a cylindrical/conical shell with a tangential feed and two axial exits. A typical hydrocyclone is shown in Figure 2.1. The tangentially injected feed has sufficient velocity to create a vortex action. As the rapidly rotating liquid spins about the axis of the cone it is forced to spiral inward and out through one of the axial exits. The rotation of the fluid causes a centrifugal force field to move solid particles toward the wall. Viscous forces resist this motion and thus particle size and density are both important factors in separation. Larger, heavier particles of solid are thrown outward against the wall and spiral downward to exit at the apex of the cone with the underflow. Smaller particles may remain in the liquid as it spirals inward and upward to be discharged with the overflow. The spiraling pattern can be seen in Figure 2.1.

Hydrocyclones are generally used when the particles to be removed are between 5 and 700μ. A density differential between the solids and the liquid of 2.7 is also desired but not essential.

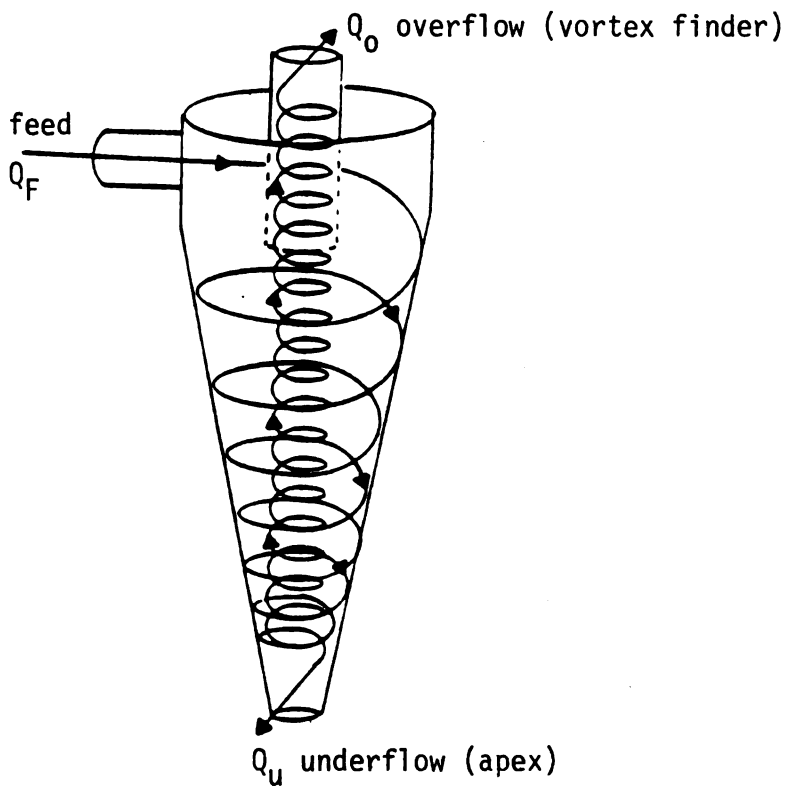

Figure 2.1. A typical hydrocyclone and its flow pattern

The cleaning of pulp stock prior to the making of paper, the separation of coal from shale, the recovery of catalyst from the cracked oil of a fluidized bed cracking unit are a few of the many important industrial applications mentioned by Bradley [1965]. Typically, hydrocyclones are used to recover fine coal particles, less than 0.025", from denser impurities by using water as a separating medium. Considering that more than half of the coal mined in the United States is beneficiated and approximately 15-20% of this is lost due to inefficient coal preparation methods, a quick and easy way to recover some of the more than 1 billion tons of refuse coal (see Schmidt and Hill, 1976) would be to improve the performance of hydrocyclones.

Hydrocyclones used to separate solids from liquids are known as thickeners. The range of particle sizes most common in these applications is 5 to 200 microns. Settling velocities of particles smaller than 2 microns are too low [Bradley, 1965] to permit efficient separation even under the high centrifugal forces which exist in small cyclones. The range of values of centrifugal acceleration in the 10mm hydrocyclone are 500 to 30,000 times the acceleration due to gravity and possibly even higher. Because of the magnitude of this centrifugal acceleration, the effect of gravity can easily be neglected and hydrocyclones can be operated in either a horizontal or vertical position.

Hydrocyclones can also be used to separate according to particle size, density and shape. This is called classification. Here, the hydrocyclone is not designed to be efficient for all

sizes, shapes or densities of solids. Instead, use of a "cut point" is made. Particles with densities, sizes or shapes below the cut point are poorly separated. Particles above the cut point are separated with a high degree of efficiency (see Section 2.1.3).

2.1.1 Capacity

The capacity of a hydrocyclone is determined by the pressure drop across the unit. The pressure drop is defined as the pressure difference between the feed stream and the overflow stream. This is the most convenient due to the normal predominance of the overflow rate over the underflow rate and the fact that the overflow in many applications remains the process stream. Pressure drop in this case includes entry and exit losses.

A number of papers have attempted the theoretical approach of fluid mechanics with the intention of deriving general relationships from momentum balances for hydrocyclones. These are unfortunately very complex and include, from integration operations, two or three constant coefficients, which have to be determined empirically, despite some simplifying assumptions intended to bypass the mathematical difficulties.

Many workers adopted the pragmatic approach of correlation, changing one factor at a time and trying to isolate its effect. Because of the large number of variables and their mutual interaction, this method was limited to narrow ranges of variables and led to inconsistent results (see Dahlstrom, 1949; and, Hatschke and Dahlstrom, 1958).

On a more simplistic view, the total flow rate, Q_F, can be related to the operating pressure drop, ΔP, by the following equation:

$$Q_F = K(\Delta P)^X \qquad (2.1)$$

where K depends on each new design. Although this formula is severely limited to a particular hydrocyclone fluid and solid system, it has one major advantage. By plotting Q_F versus ΔP on a log-log plot, the values of K and X are easily determined.

The value of X should be relatively independent of the particular hydrocyclone and thus comparison with other results is meaningful. Table 2.1 gives a list of the exponent values obtained by others. Note the good agreement shown for various size hydrocyclones. Also, it is interesting to observe that as the hydrocyclones decrease in size the value of the exponent increases.

TABLE 2.1.--Values of 'X' for Various Size Hydrocyclones

Source	Size (D_c)	Exponent (X)
Kelsall [1953]	3 inch	0.416
Bradley & Pulling [1959]	3 inch	0.425
Mitzmager & Mizrahi [1964]	3-15cm	0.430
Pilgrim & Ingraham [1962]	3 and 15mm	0.452
Haas, et al. [1957]	0.50 - 0.16 inch	0.44
Wallace [1980]	10mm	0.46

Moder and Dahlstrom [1952] did an extensive study on 3 to 7 inch hydrocyclones. They used a value of 0.5 for X and concluded that K should be broken up into two parts. These parts included a new proportionality factor, K', which was a function of the design variables and the product of the inlet diameter and the overflow diameter to the 0.9 power. Further, it was determined that K' was dependent on the split ratio and the ratio of the inlet to overflow diameters.

Another important parameter that affects the capacity of a hydrocyclone is the feed stream viscosity. Even though a viscosity term does not enter into the relationship for pressure drop, an increase in viscosity nevertheless causes a decrease in pressure drop for the same flow rate (see Bradley, 1964, p. 142). Therefore, K in Equation (2.1) is also dependent on viscosity. Fontein, et al. [1962] also observed that a rise in viscosity produces a higher capacity at the same pressure drop. They gave the following explanation for this phenomenon. The medium is fed tangentially at the circumference of the cyclone and is discharged at a short distance from the center. Besides the rotational flow there is also a radial, inwardly-directed flow which is counteracted by the centrifugal force. At the same feed (tangential) velocity at the wall of the cyclone a rise in the viscosity of the medium reduces the tangential velocity at a radius smaller than the wall which means there is a lower pressure drop. In other words, the tangential velocity profile is flattened. The decrease in pressure can also be shown

mathematically if we assume that at least part of the pressure loss is due to a radial pressure gradient in the tangential velocity.

2.1.2 Split Ratio

In phase separation applications, such as solid from liquid, or even liquid from liquid, where the object is to obtain the separate phases as free as possible from each other, it is obviously of considerable importance to split the feed into the right volumetric proportions. The term split ratio refers to the overflow rate divided by the underflow rate.

Moder and Dahlstrom [1952] developed a relationship for large diameter hydrocyclones that showed a dependence on the underflow and overflow diameters as well as the volumetric flow rate. The relationship showed an increase in the split with an increase in the flow rate with an exponent value of 0.44. Many other relationships for various size hydrocyclones showed no dependence on the flow rate (see Bradley, 1965, pp. 102-104). The dependence was based solely on the ratio of the underflow to overflow diameters.

Experimental data from several sources indicate that the split ratio is indeed a weak function of the flow rate. Rietema [1961] has data for a small 3" hydrocyclone with an overflow to underflow diameter ratio of 1 that show a 50% increase in the split for a tenfold increase in the operating pressure. Haas, et al. [1957] have data for 10mm and smaller hydrocyclones that indicate the split is independent of the flow rate. Kelsall [1953] did experiments with a 3 inch hydrocyclone with $D_o/D_u >> 1$ and saw only

a small increase in the split with increasing flow rate. Additionally, Bradley [1965, pp. 103-104] stated that his work with small hydrocyclones as well as that of others showed conditions where the split decreased, was constant, or increased with an increase in flow rate. Also, the volume split was independent of feed diameter, cyclone diameter, vortex finder external dimensions and wall roughness. Balanced back pressure conditions resulted in the same split as for free discharge.

Viscosity of the feed stream also has an effect on the split. Bradley [1965, p. 143] shows that an increase in viscosity causes the split ratio to decrease. This decrease is most dramatic in the range of 1-10 cp for feed viscosity.

2.1.3 Efficiency

Defining an efficiency for the hydrocyclone is difficult. A single number is not capable of fully describing the results of a separation unless it is ideal. A hydrocyclone not only has to deliver solid as free from liquid as possible in the underflow but also has to remove as much solid from the liquid as possible in the overflow. Van Ebbenhorst Tengbergen and Rietema [1961] do an excellent job of explaining this concept and summarizing the equations found in the literature. The efficiency used in this research is taken from Kelsall [1953] but this definition is a variation of the form recommended by van Ebbenhorst Tengbergen and Rietema [1961]. The centrifugal efficiency is defined as the solids found in the underflow due to the centrifugal separation

force divided by the total solids capable of being affected by the centrifugal force. The basic assumption here is that the feed splits into two internal streams when it is introduced into the hydrocyclone. One of these streams accounts for all the liquid found in the underflow and the other for all the liquid found in the overflow. Both streams have the same solids concentration as the feed. Hypothetically, this is the result expected if no centrifugal forces were present in the hydrocyclone. Next, it is assumed that the centrifugal forces act only on the solids in the "overflow" stream and remove some of them to the "underflow" stream. It should be realized that this definition does not account for any particles that may be driven from the underflow stream to the overflow stream. Also, it does not account for any portion of the overflow that short circuits to the vortex finder and thus is never influenced by the centrifugal forces.

Figure 2.1 expresses the foregoing idea schematically. Here W_F, W_o and W_u represent the mass flow rates and X_F, X_o and X_u represent the mass fraction of solids in the feed, overflow and underflow streams, respectively. W_o^* and W_u^* are the resultant streams when the internal split takes place and contain the same mass fraction of solids as the feed stream, X_F. These streams do not actually exist separately within the hydrocyclone but are merely used to illustrate the definition of the centrifugal efficiency, viz.,

$$E = \frac{W_s^*}{X_F W_o^*} . \qquad (2.1)$$

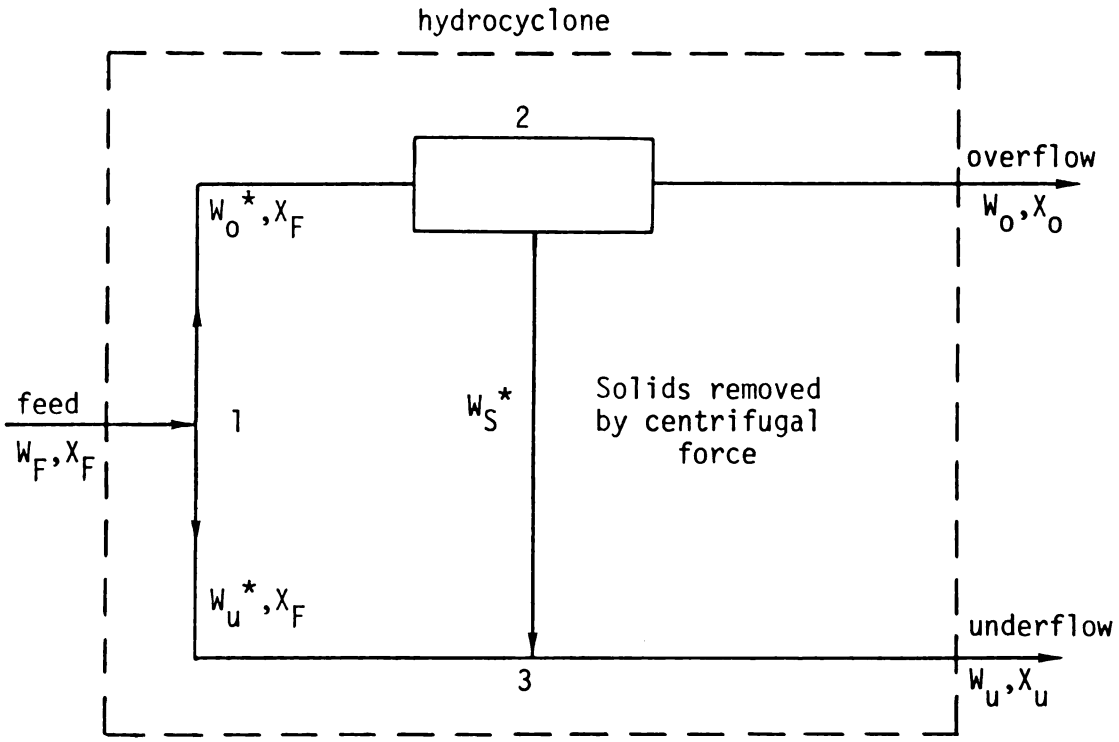

Figure 2.2. A schematic of the definition of centrifugal efficiency used in this study.

Obviously, W_o^* and W_s^* cannot be observed directly but these parameters can easily be related to measured ones by using component material balances.

A solids balance around control volumes 1 and 3 (see Figure 2.1) gives, respectively,

$$X_F W_o^* = X_F W_F - X_F W_u^* \tag{2.2}$$

and

$$W_s^* = X_u W_u - X_F W_u^* . \tag{2.3}$$

Therefore, Equation (2.1) can be expressed as

$$E = \frac{X_u W_u - X_F W_u^*}{X_F W_F - X_F W_u^*} . \tag{2.4}$$

Now W_u^* can be determined by a water balance around control volume 3 inasmuch as all the underflow liquid by assumption comes from W_u^*. Therefore, with

$$(1 - X_F)W_u^* = (1 - X_u)W_u, \tag{2.5}$$

the centrifugal efficiency, defined by Equation (2.1), can be calculated in terms of measured variables.

The efficiency of a hydrocyclone is affected by the fluid viscosity, differences in the solid and fluid densities, the particle's size and shape and, obviously, the centrifugal force generated inside the hydrocyclone. Moreover, because most solids to be

separated are not monodisperse, the size distribution is also an important characteristic of the solids.

2.2 Polymer

The polymer used in these experiments was Separan AP-30 manufactured by the Dow Chemical Company (Midland, Michigan). It is a high molecular weight polymer (~1-3 million) made by polymerizing acrylamide and carboxyl groups in a 3 to 1 ratio as shown in Figure 2.3. The amide groups are essentially nonionic in solution although a small number (<0.5%) will hydrolyze to form an anionic carboxyl group. The anionic nature of the polymer is determined by the carboxyl group. In neutral or alkaline solution the polymer is classified as an anionic polyelectrolyte. However, under acidic conditions the ionization is repressed and the electrolyte assumes a nonionic character.

Separan AP-30 was chosen for several reasons. It is soluble in water, although care must be taken to avoid clumping, and the polymer is not poisonous. The monomer unit however is highly toxic. Separan is also a known drag reducing agent and is difficult to completely degrade. One drawback, however, is the fact that it is a well-known flocculating agent and thus tends to agglomerate particles in solution.

A straight chain Separan AP-30 molecule is ~4.1μ in length depending on the molecular weight of that particular chain. Typically, the concentration of clay and polymer are both 100 wppm. This produced a ratio of ~1 x 10^6 polymer particles per clay particle. This means that there are one million polymer chains to

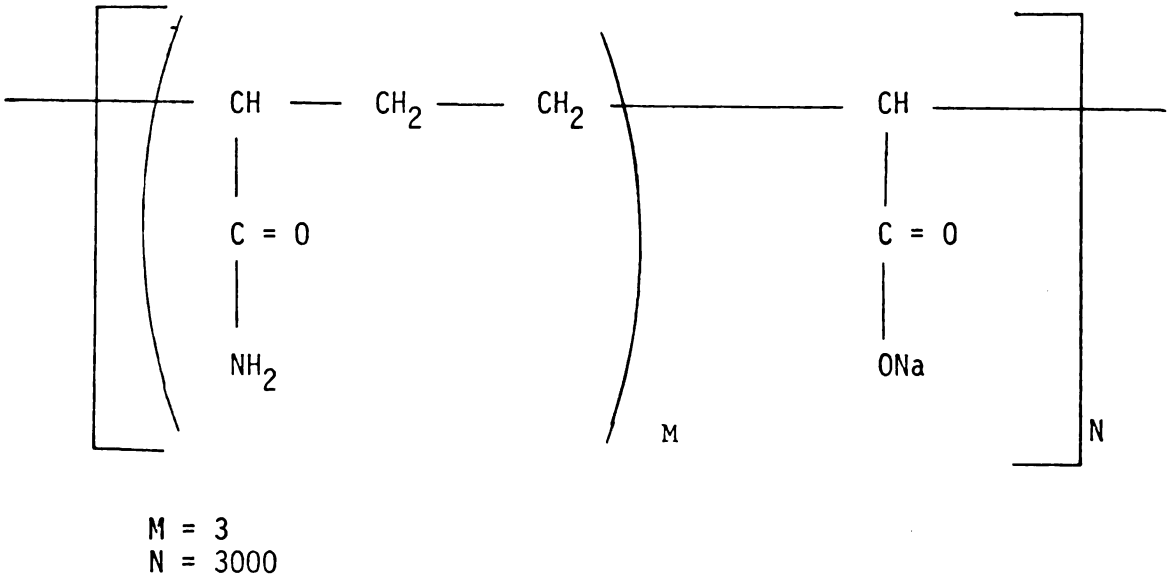

M = 3
N = 3000

Figure 2.3.--The Chemical Structure of Separan AP-30

agglomerate each clay particle. Since the clay particles are on the average ~1μ in diameter, the clay particles see an endless sea of sticky polymer chains and very few clay particles. The conditions are good for flocculation to occur.

2.3 Clay

The information contained herein on the clay is designed to give the reader some background on the mechanism of flocculation between kaolinite clays and Separan AP-30. Evidence that flocculation could occur in this research project is discussed here. This flocculation could have a severe effect on the outcome of this research and needs to be considered carefully because agglomerated particles are larger than the individual clay particles and are easier to separate in the hydrocyclone.

The clay used in these experiments was furnished by the Georgia Kaolin Company. It is a kaolinite clay which has a median particle size of ~1μ. Typically, a chemical analysis yields 38% Aluminum Oxide, 45% Silicon Dioxide, 14% water and some trace elements.

Clays are classified into two main groups, structured and amorphous (see Hillel, 1980). The structured clays are subclassified according to their internal structure into two principal types, 1:1 and 2:1 minerals. The ratio indicates the relative number of tetrahedral to octahedral sheets in the structure. The most

common mineral within the 1:1 type is the kaolinite, which is used in this research.

The basic layer in the crystal structure, as shown in Figure 2.4A is a pair of silicon-alumina sheets, and these are stacked in alternating fashion and held together by hydrogen bonding in a rigid, multilayered lattice which often forms hexagonal platelets. Since water and ions cannot enter between the basic layers, these cannot ordinarily be split. Moreover, since only the outer faces and edges of the platelets are exposed, kaolinite has a rather low specific surface. This means that the area available for polymer interaction is lower than in other clays.

Kaolinite crystals generally range in planar diameter from 0.1 to 2μ with a variable thickness of 0.02 - 0.05μ. Owing to its relatively large particles and low specific surface, kaolinites exhibit less plasticity, cohesion, and swelling than most other clay minerals. The unit layer formula is $A\ell_4\ Si_4\ O_{10}\ (OH)_8$ and it has a specific gravity of 2.8.

When a colloidal clay particle is more or less dry, the neutralizing counterions are attached to its surface as in Figure 2.4B. Upon wetting, however, some of the ions dissociate from the surface and enter into solution (see Figure 2.4C). A hydrated clay particle therefore forms a micelle, in which the adsorbed ions are spatially separated, to a greater or lesser degree, from the negatively charged clay particles. The negative charge of the clay particles in solution was confirmed by a simple experiment (see Chapter 4). Together, the particle surfaces acting as a multiple

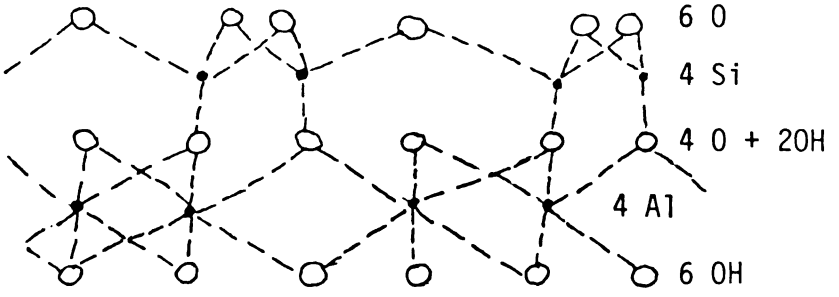

$Al_4Si_4O_{10}(OH)_8$

A

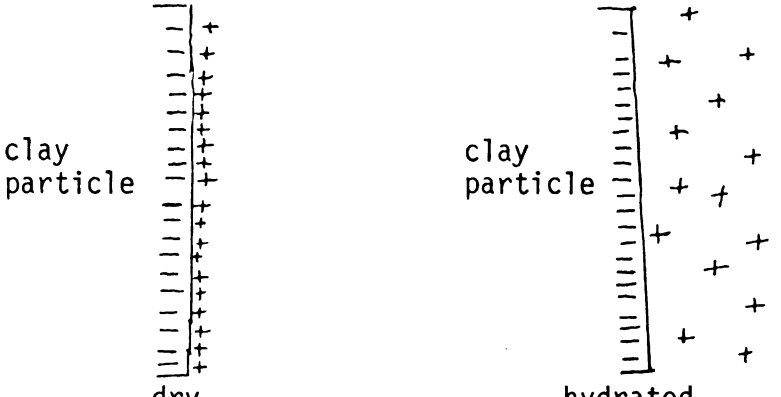

B C

Figure 2.4. The structure of kaolinite clay (A, the basic crystal structure for kaolinite clay; B, a dry clay particle showing the "double layer"; C, a clay particle in the hydrated state).

anion, and the "swarm" of cations hovering about it, form what is known as an electrostatic double layer. The actual concentration of cations inside the double layer can be 100 or even 1,000 times greater than in the solution.

The cations in the "double layer" can be replaced or exchanged by other cations in solution. The cation exchange capacity, the total number of exchangeable cation charges, is a commonly reported parameter. This phenomenon affects flocculation and dispersion of kaolinite in solution. With and without polymer, kaolinites have the lowest exchange capacity of all the clays (only 13 me/100 gms*).

Greenland and Hayes [1978] suggested that the reason kaolinites have such low exchange capacities is that the surfaces of the crystals are uncharged and the observed charges occur only at the crystal edges where the silanol and aluminol groups are incomplete.

Michaels and Morelos [1955] investigated the adsorption and flocculation of sodium polyacrylate and polyacrylamide on kaolinite. They concluded that adsorption of these anionic polyelectrolytes on kaolinite in all prcbability occurs via hydrogen bonding between the unionized carbonyl/anoxide groups on the polymer chains and oxygen atoms on the solid surface. Adsorption is hindered by electrostatic repulsion between negatively charged clay surfaces and the carboxyl groups on the polymer (see Figure 2.5). Intramolecular association between hydrogen bonding groups on a polymer chain

*me stands for milliequivalents which is one mole of hydrogen or any ion which can combine with or replace the exchange cations.

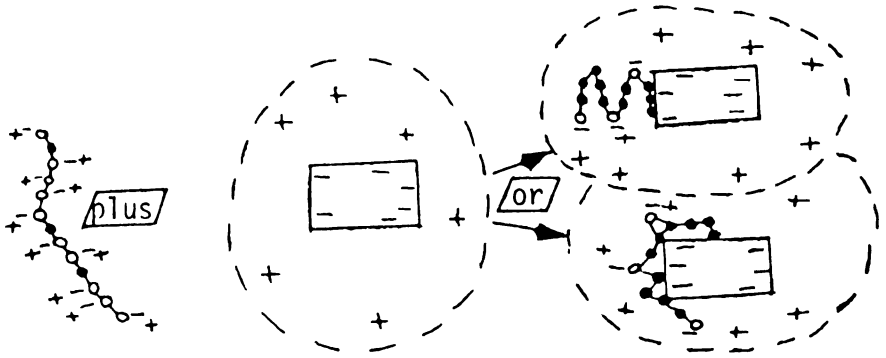

A. Adsorption of sodium polyacrylate by kaolinite.

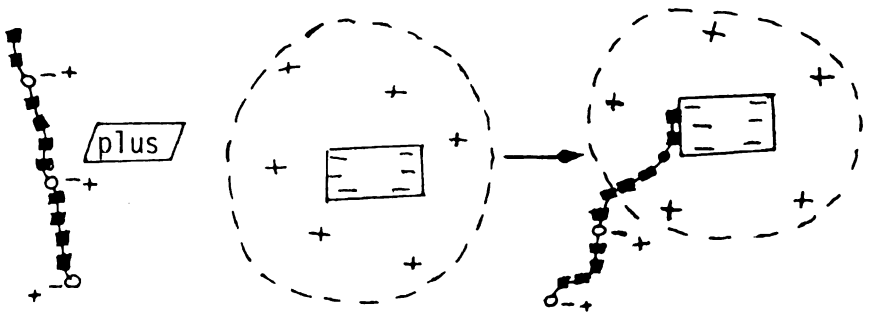

B. Adsorption of polyacrylamide by kaolinite.

Figure 2.5. Mechanism of adsorption of polyelectrolytes on kaolinite (schematic from Michaels and Morelos, 1955).

● = Carboxyl (COOH)

○ = Carboxylate (COO^-)

■ = Amide ($CONH_2$)

evidently is competitive with the adsorption of these groups by kaolinites. For polymers rich with active hydrogen bonding groups as in sodium polyacrylate, the intramolecular association tendency is so great that the opportunity for adsorption is significantly reduced. With polymers containing less active hydrogen bonding such as polyacrylamide, the extent of intramolecular association is lower and the adsorption of such compounds by kaolinite is limited primarily by the number of active bonding sites on the solid surface.

Adsorption of anionic polyelectrolytes by kaolinites is not necessarily accompanied by flocculation. Flocculation is caused by bridging of solid particles by polymer molecules and is controlled by the configuration of the molecule in the adsorbed state. For polyelectrolytes, molecular configuration is determined by the degree of intramolecular association which favors the coiling and the extent of ionization which favors chain extension. Under high pH conditions, where polymer adsorption by kaolinites occurs, anionic polyelectrolytes nevertheless cause flocculation by the same mechanism as that of simple electrolytes.

CHAPTER 3

EXPERIMENTAL APPARATUS

3.1 Flow Loop

A schematic of the entire flow loop is shown in Figure 3.1. The overflow and underflow can both be individually throttled to change the back pressure. Two centrifugal pumps (Myers, QP30-3) connected in series provided a feed flow rate to the hydrocyclones with pressures up to 98psi at the inlet. A bypass that recycles some of the flow from the high pressure side of the pumps was used to provide flow control and tank agitation. A copper tube was coiled and placed in the reservoir for temperature control. It proved to be excellent at maintaining the temperature at any value between 15-30°C depending on ambient air temperature and on cooling water temperature. All piping is copper with one inch (2.54 cm) I.D. connected directly to the tank and pumps and with 1/2 inch (1.27 cm) going to the bypass, hydrocyclone and drag reduction section.

The holding tank was operated at 2/3 capacity or 154ℓ during the experiments. The bypass was used to mix the tank contents. Samples taken at the top and the bottom of the tank were compared during the separation runs and were shown to have the same solids concentration.

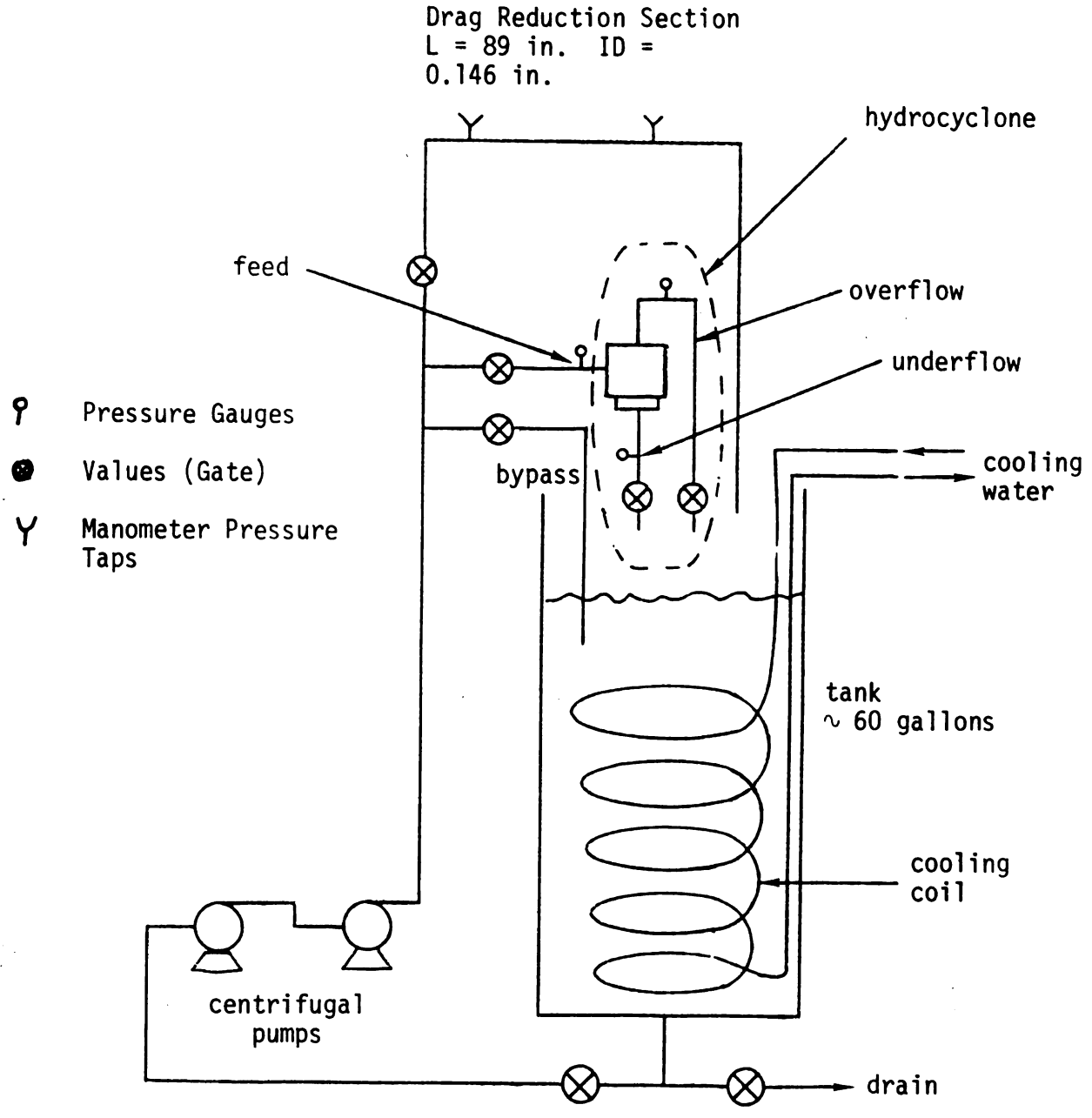

Figure 3.1. Schematic of experimental flow loop.

The pressure gauges were located 6" from the hydrocyclone. Locating them closer caused too much fluctuation in their readings. The feed pressure gauge reads 0-100 psig while the overflow and underflow gauges read 0-60 psig.

3.2 The Hydrocyclone

The hydrocyclone separator used is actually a cluster of six 10mm hydrocyclones marketed by Dorr-Oliver as an impurity eliminator. The parallel operation of the cluster can be seen in Figure 3.2. It is important to note the common manifolds present at the overflow and underflow streams. This design feature may influence some of the operating characteristics in a manner not observed for other hydrocyclones.

Figure 3.3 shows the nominal dimensions of the 10mm hydrocyclone studied. Also shown are the "optimal" scale ratios recommended by Rietema [1961]. The connections made between the cluster of hydrocyclones and the flow loop are shown in Figure 3.4. The location of control valves and pressure taps is an important detail in designing the experiment.

A more intuitive idea of the specific apparatus used follows by examining the two photographs presented in Figure 3.5.

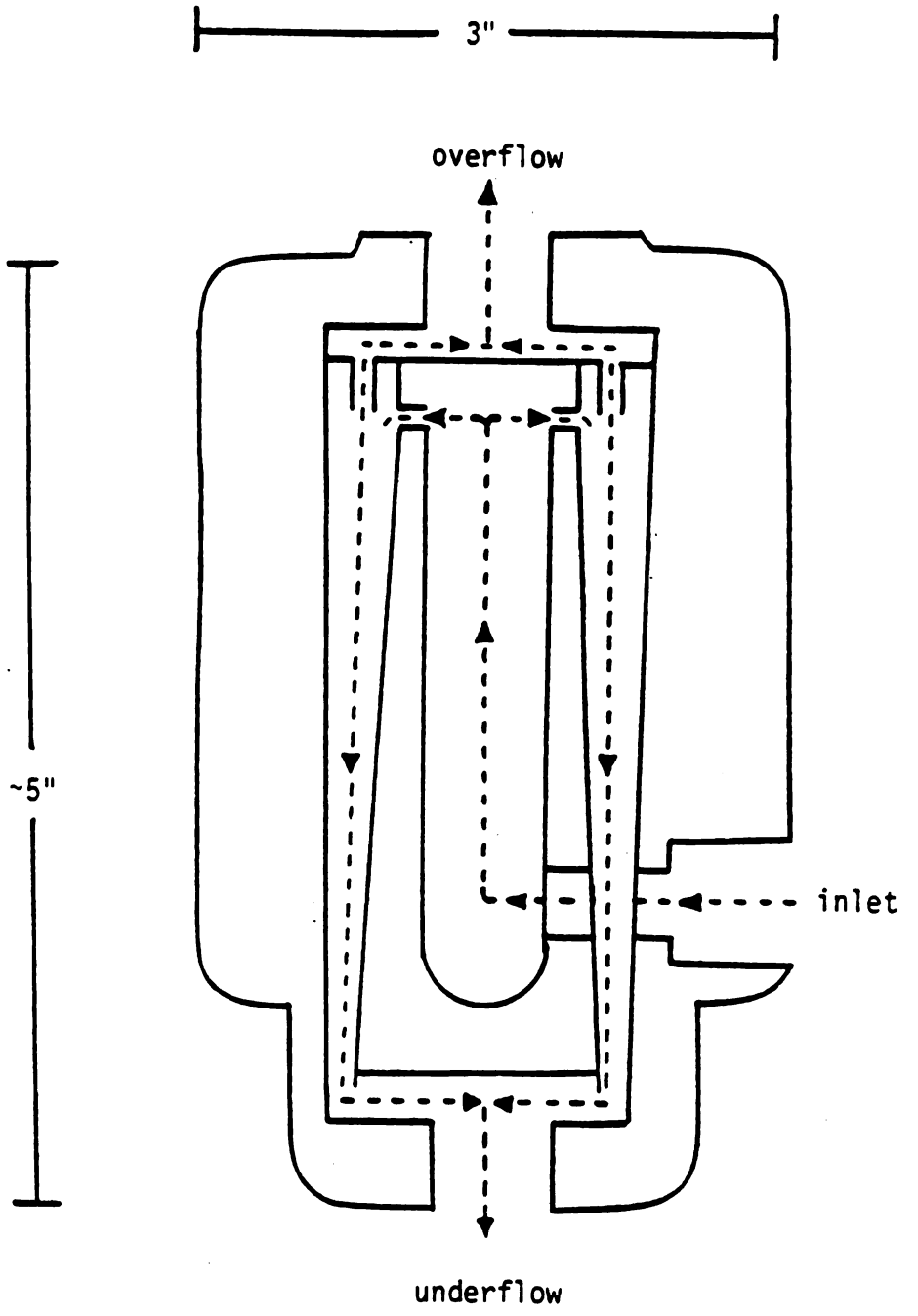

Figure 3.2. Flow through a manifold of six 10mm hydrocyclones

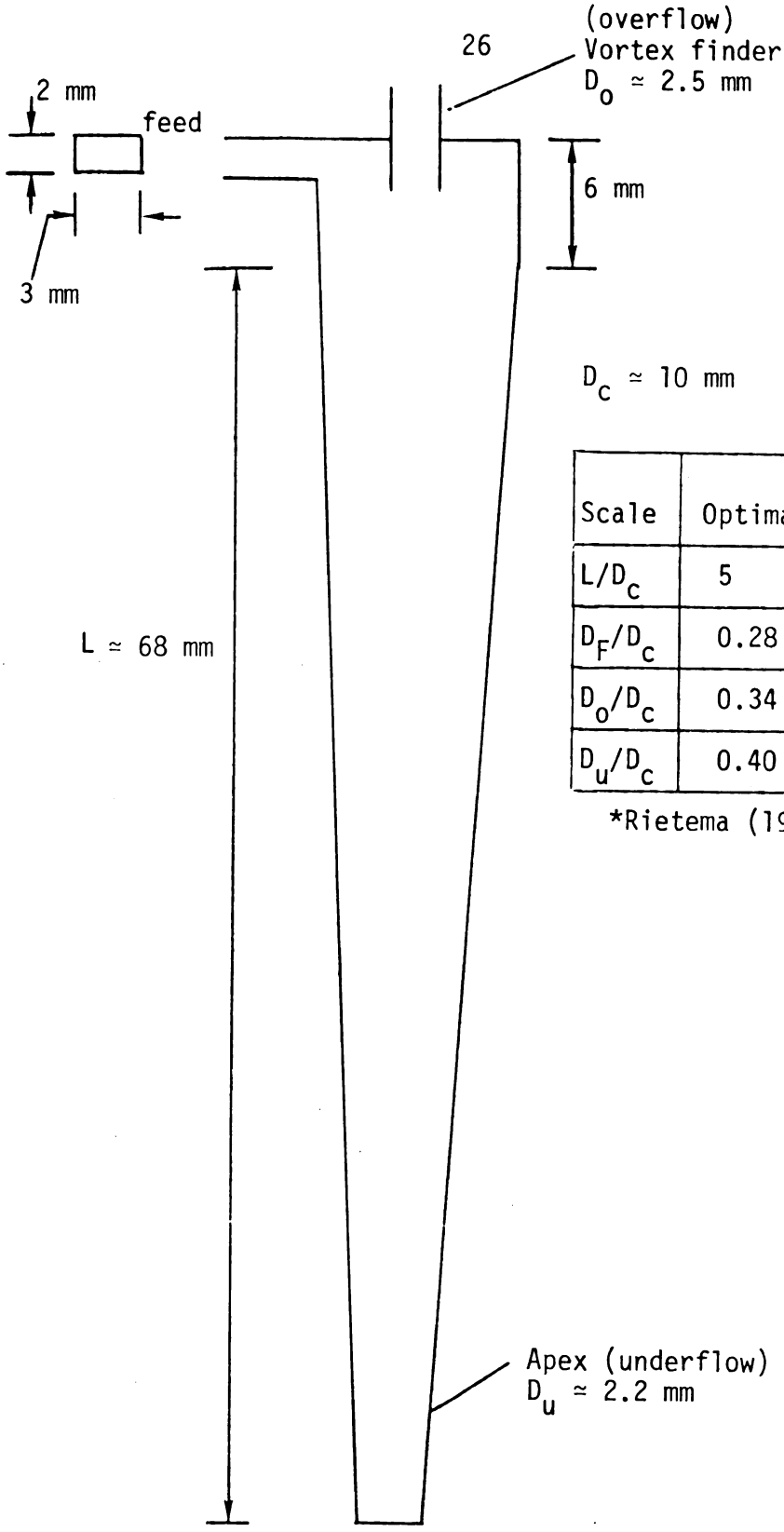

Scale	Optimal*	Doxie 5 Dorrclone
L/D_c	5	7.4
D_F/D_c	0.28	0.24
D_o/D_c	0.34	0.25
D_u/D_c	0.40	0.22

*Rietema (1961)

Figure 3.3. Nominal dimensions of the Doxie 5 Dorrclone.

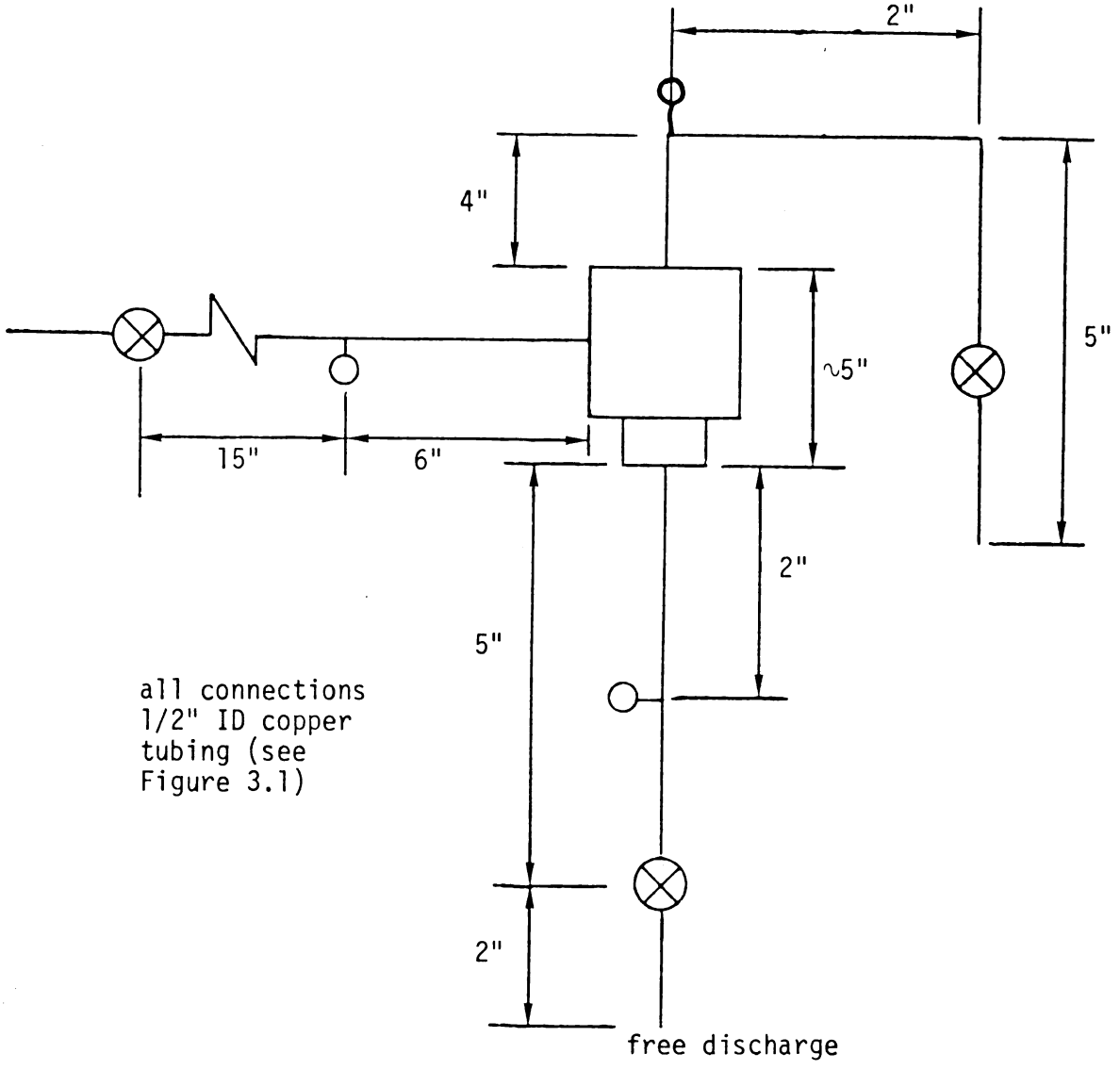

Figure 3.4. Connection of the Dorrclone with the flow loop.

Figure 3.5. Photographs of the Dorrclone connections and cluster design.

CHAPTER 4

EXPERIMENTAL PLAN AND PROCEDURE

This chapter contains the details of procedures used to determine how different mixing strategies affect the hydrocyclone split ratio and centrifugal efficiency for a suspension of kaolinite clay and Separan AP-30. The effects of polymer degradation due to the pumps in the flow loop will also be investigated indirectly by examining the drag reduction characteristics of the various polymer-water-clay mixtures (see Appendix A). In general, the mixing strategy had little effect on the apparent viscosity, drag reduction, and split ratio, but affected the separation efficiency considerably. Mechanical degradation by the pumps also had a significant effect on the split ratios and separation efficiency (see Chapter 5).

An earlier study by Wallace [1980] showed that the order in which the clay and polymer were added to solution turned out to be quite important in determining the separation efficiency. Thus, two well defined mixing strategies (I and II) were employed throughout this study. Table 4.1 gives a summary of the various recipes used which are quite simple and easily reproducible.

Mixing strategy I consisted of sprinkling the polymer in its dry form onto the surface of the water in the holding

TABLE 4.1.--Mixing Strategies Studied

Mixing Strategy	Procedure Followed to Prepare a Final Suspension of 100 wppm Polymer and 0.2 wt. % Clay
I	1) Close all valves and add 154ℓ of tap water to the mixing tank. Let stand overnight to come to room temperature.
	2) Close valves 1 and 2 (see Figure 3.1). Open valve 3 and start the pumps. Start cooling water and adjust tank to desired temperature gradually.
	3) Add 15.4 grams of dry Separan AP-30 by sprinkling it into the tank slowly. This takes 15-30 seconds.
	4) Add 308 grams of dry kaolinite clay immediately after step 3.
	5) Start taking data immediately.
II	Repeat steps 1 and 2
	3) Add 308 grams of dry kaolinite clay.
	4) Add 15.4 grams of dry Separan AP-30 by sprinkling it into the tank slowly.
	5) Start taking data immediately.
III	Repeat steps 1 and 2
	3) Shut off pumps, stir the fluid in the holding tank by using a turbine at a low speed.
	4) Add 15.4 grams of dry Separan AP-30 by sprinkling it into the tank slowly.
	5) Add 308 grams of dry kaolinite clay.
	6) Stir for one minute. Start pumps.
	7) Start taking data immediately.

TABLE 4.1.--Mixing Strategies Studied (continued)

Mixing Strategy	Procedure Followed to Prepare a Final Suspension of 100 wppm Polymer and 0.2 wt. % Clay
IV	Repeat steps 1 and 2
	3) Add 15.4 grams of dry Separan AP-30 by sprinkling it into the tank slowly.
	4) Allow the solution to circulate through the bypass for 30 minutes.
	5) Add 308 grams of kaolinite clay suspended in 1-2 gallons of tap water.
	6) Take data immediately.

tank while the pumps were cycling the fluid around the flow loop (see Figure 3.1). Immediately after all the polymer was added, dry clay was sprinkled into the fluid. This whole process took approximately 60 seconds.

The second strategy (II) is simply the reverse of the first. Dry clay is dispersed into a large tank of water and allowed to mix for a few minutes. The polymer (dry) is then sprinkled into the clay-water suspension. In both cases (I and II), the pumps continuously mix the fluid by cycling it through the bypass line shown in Figure 3.1. Obviously, the intense mixing through two centrifugal pumps may cause significant degradation of the high molecular weight polymer. Therefore, two additional mixing protocols (III and IV) were followed for some of the separation studies presented in Section 5.3.

In the third mixing strategy the shearing of the polymer was minimized by stirring the water in the holding tank by using a turbine at a very low speed. The clay was added after the polymer

was well mixed and then the pumps were turned on and the separation experiments started immediately. Another variation of this involved hand mixing of the polymer and water. The solution was allowed to sit overnight before adding clay. All mixing was done by hand without the use of the pumps or the turbine. Efficiency data for this mixing strategy were taken at constant pressure drop to investigate its transient behavior (see Figure 5.15).

In the fourth mixing strategy, the polymer was subjected to the high shearing available in the pumps for 30 minutes prior to the addition of the clay. Clay was added in solution rather than in its dry form. In this particular run, an additional amount of polymer was added after 9 minutes to determine its effect on the efficiency (see Figure 5.16).

The first two mixing strategies were the only procedures used when investigating the viscosity, drag reduction, and hydrocyclone characteristics. All the mixing strategies were used in the separation experiments in an attempt to exploit or eliminate the mechanical degradation of the polymer.

Samples of all the mixing strategies were obtained for visible inspection. These were taken before, during, and after the completion of the experiment. Visibly, no differences in the solutions were noted except in the low shear mixing strategy. This suspension contained large flocs (0.25") after the addition of the clay to the polymer solution which almost instantaneously disappeared when the pumps were engaged. The suspension then turned milky white and was identical to all the other clay/

polymer suspensions studied. Comparing solutions obtained before the data were taken and after the experiment was completed showed no visible differences. Thus, at first glance it is not possible to tell if flocs are forming and changing in size.

Solution pH and temperature were both monitored continuously. The temperature fluctuated occassionally but rarely by any significant amounts. The pH of the solutions studied was independent of polymer and/or clay concentrations in the range investigated. The charge on the clay particles suspended in water was negative, which was verified by connecting a battery (1.5 volts) to two copper wires suspended in an aqueous solution of clay. Clay particles collected on the positive copper wire while nothing collected on the cathode, even after one week.

The operating characteristics of the hydrocyclone used in this research are carefully mapped out. The capacity and split ratio (Qo/Qu - see Notation) were studied for different polymer-water-clay mixtures. The split ratio and capacity measurements were done by weighing and timing the overflow streams. The total flow was assumed to be equivalent to the sum of the overflow and underflow. Pressure drops were recorded up to 98 psig for the feed stream. The underflow and overflow back pressures were also measured. Example experimental data are recorded in Appendix B in tabular form, and the results are discussed in Chapter 5. Table 4.2 defines the range of parameters investigated.

Four separation experiments were conducted on 0.2 wt % clay suspensions (see Table 4.1). The first two experiments used

TABLE 4.2.--Parameters Investigated in This Study.

Parameter	Range Investigated
Temperature	15°C, 25°C
Polymer concentration (Separan AP-30)	0-300 wppm mainly 100 wppm
Clay concentration (Georgia Kaolinite)	0-2 wt % mainly 0.2 wt %
Hydrocyclone feed pressure	10-98 psig
Flow rate (six hydrocyclones)	2.40-6.60 gpm
Entrance velocity to one 10mm hydrocyclone	95-260 ft/sec 65-180 mph 29-78 m/sec
Reynolds Number Based on Inlet Conditions	1.5×10^4 - 3.5×10^4

both mixing strategies I and II and contained 100 and 200 wppm AP-30, respectively. In the third experiment the mixing of the polymer was done using a stirring motor in the hopes that the effect of shearing would be minimized. In the final experiment, the polymer was recycled through the pumps for 30 minutes in order to shear the polymer as much as possible. Specific details on the mixing of the solutions are listed in Table 4.1.

To measure the separation efficiency of the hydrocyclone the clay concentration of the feed, overflow, and underflow streams as well as their flow rates are required. The flow rates were measured by timing and weighing an amount collected from the desired stream. The feed stream was assumed to be equal to the

sum of the overflow and underflow streams. To measure the clay concentration a sample of the desired stream was taken and weighed. The sample was then dried out in an oven overnight and the remaining clay was weighed. The feed stream concentration was measured in two different ways. The first method involved taking a sample from the holding tank and the second method involved collecting the overflow and underflow streams in the same container. The two methods produced results that agreed to within 1%. This showed that mixing in the tank was uniform.

All efficiency runs were subject to verification by doing a mass balance on the hydrocyclone system. All mass balances closed to within 4% and more than half closed to less than 1%.

In all but one of the experiments, the data were collected by either increasing or decreasing the Reynolds number based on the hydrocyclone feed stream which ranged from 18,000 to 34,000. A base line using no polymer was established for comparing the effects due to polymer additives.

CHAPTER 5

RESULTS AND DISCUSSION

5.1 Flow Characteristics Without Polymer Additives

Figure 5.1 shows the effect of pressure drop on the capacity of six 10mm hydrocyclones (see Section 3.2 for a detailed description of the Doxie 5 Dorrclone). The back pressures Po and Pu are atmospheric.

The capacity data reported by Dorr-Oliver for the Doxie 5 Dorrclone are given by the dashed line in Figure 5.1. The differences between the Dorr-Oliver and the experimental results shown here are probably due to entrance and exit connections. These are unknown for the Dorr-Oliver study but are clearly defined by Figure 3.4 for the hydrocyclone cluster investigated in this work.

The empirical correlation,

$$Q_F = 0.817\ (P_F - P_O)^{.455} \qquad (5.1)$$

developed here agrees quantitatively with an earlier study by Wallace [1980] in our laboratory and qualitatively with others summarized in Table 2.1. The exponent on the pressure drop is smaller than the usual 1/2-power dependence normally associated with high Reynolds number flow restrictions. Bradley [1965] has suggested that this is due to viscous losses related to the entrance region of the hydrocyclone. Wallace [1980], using similar

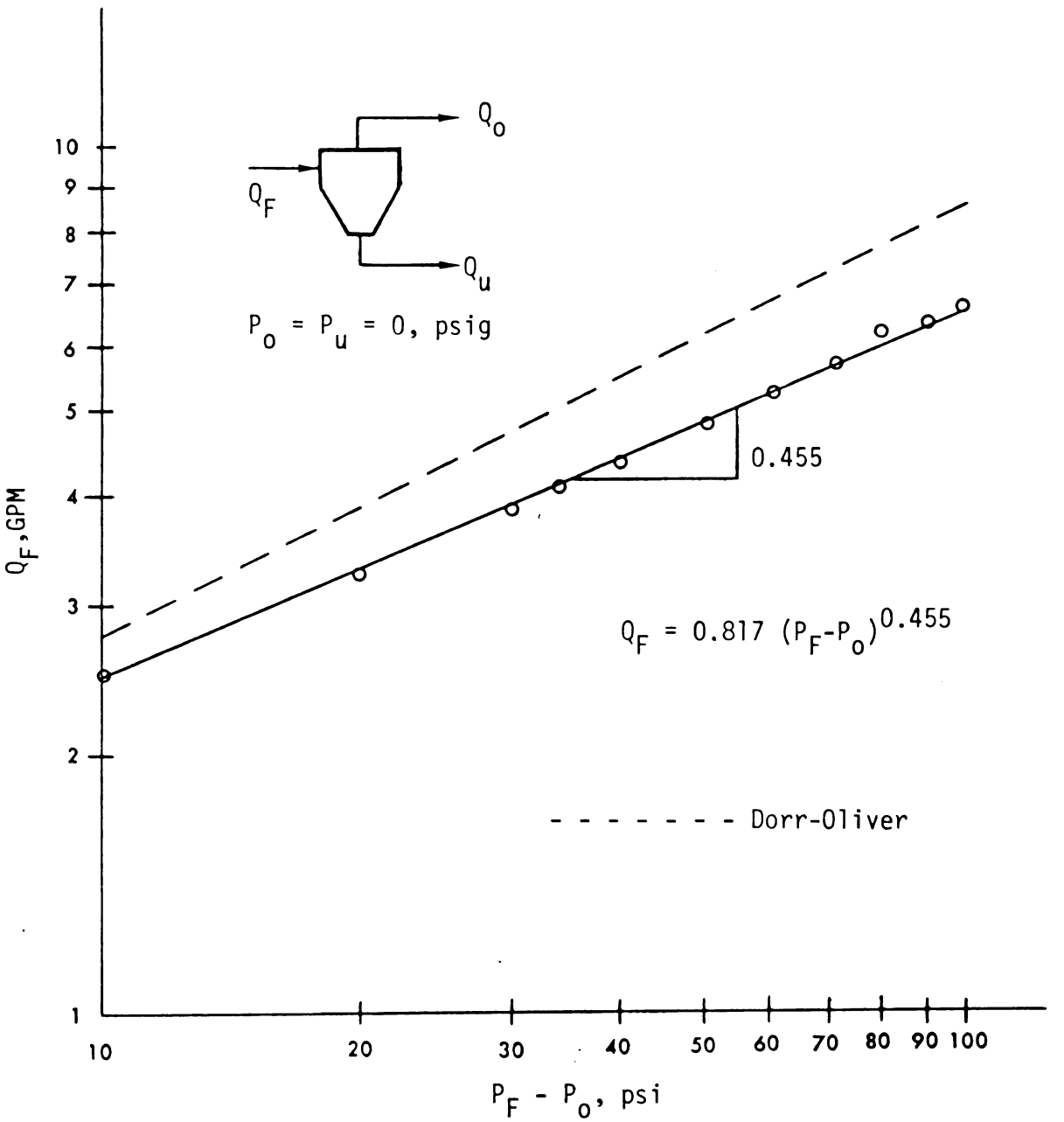

Figure 5.1. The effect of pressure drop on the capacity of six 10mm hydrocyclones (water, 25°C).

data as portrayed by Figure 5.1, assumed that the reduction in the tangential velocity at the entrance depended on the Reynolds number and showed that this could account for the exponent in Equation (5.1). Mitzmager and Mizrahi [1964] have developed a generalized correlation between the capacity and pressure drop with an exponent of 0.43; however, they note that for gas cyclones or for liquid cyclones at very high Reynolds numbers, the more conventional result obtains, viz.,

$$Q_F \propto \sqrt{P_F - P_o} \quad . \tag{5.2}$$

The effect of Reynolds number on the pressure loss coefficient defined by

$$G_o \equiv \frac{P_F - P_o}{\frac{1}{2}\rho U_F^2} \tag{5.3}$$

is shown in Figure 5.2. Mitzmager and Mizrahi [1964] have suggested that G_o should be correlated with the dimensionless group

$$N \equiv Re_F \left(\frac{D_F^2}{D_o^2 + D_u^2} \right)^{2.6} \left(\frac{D_F}{L} \right)^2 \tag{5.4}$$

where D_F, D_o, and D_u represent, respectively, the diameters of the feed entrance, vortex finder, and the apex (see Figure 3.3). L is the length of the hydrocyclone.

This study shows that the pressure drop across a single 10mm hydrocyclone is about an order of magnitude larger than the kinetic

energy of the feed stream. This is about the same pressure loss which occurs for fully developed turbulent flow in a smooth pipe with an $L/D \simeq 200$. Because a hydrocyclone operating with an air core generally shows a smaller pressure loss than one without an air core, the relative results shown in Figure 5.2 between our data and Rietema's may indicate the absence of an air core in our study.

Figure 5.2 also compares the experimental data with the centrifugal pressure loss coefficient of a free vortex having the same geometric proportions as the 10mm hydrocyclone. This simple physical model, defined by Figure 5.3, gives an upper bound on the loss coefficient for large Reynolds numbers. The model assumes that the feed velocity U_F equals the tangential velocity in the outer regions of the vortex but, actually, a smaller value should be used because of the entrance effect mentioned earlier. Therefore, the difference between the experimental pressure loss coefficient and the free vortex model at high Reynolds numbers is partly due to this phenomenon. As the Reynolds number decreases, the viscosity begins to affect the extent of velocity reduction (Wallace, 1980). Further decreases in Re_F will eventually cause G_o to reach a minimum (not shown by our data) and then increase for even lower Reynolds numbers. Below this minimum the pressure loss is dominated by viscous friction and the centrifugal loss becomes unimportant (see p. 144 in Bradley, 1965).

The split between the overflow and underflow streams is often used to control the performance of a hydrocyclone. Figure 5.4 shows how Qo and Qu depend on the pressure drop and, for the

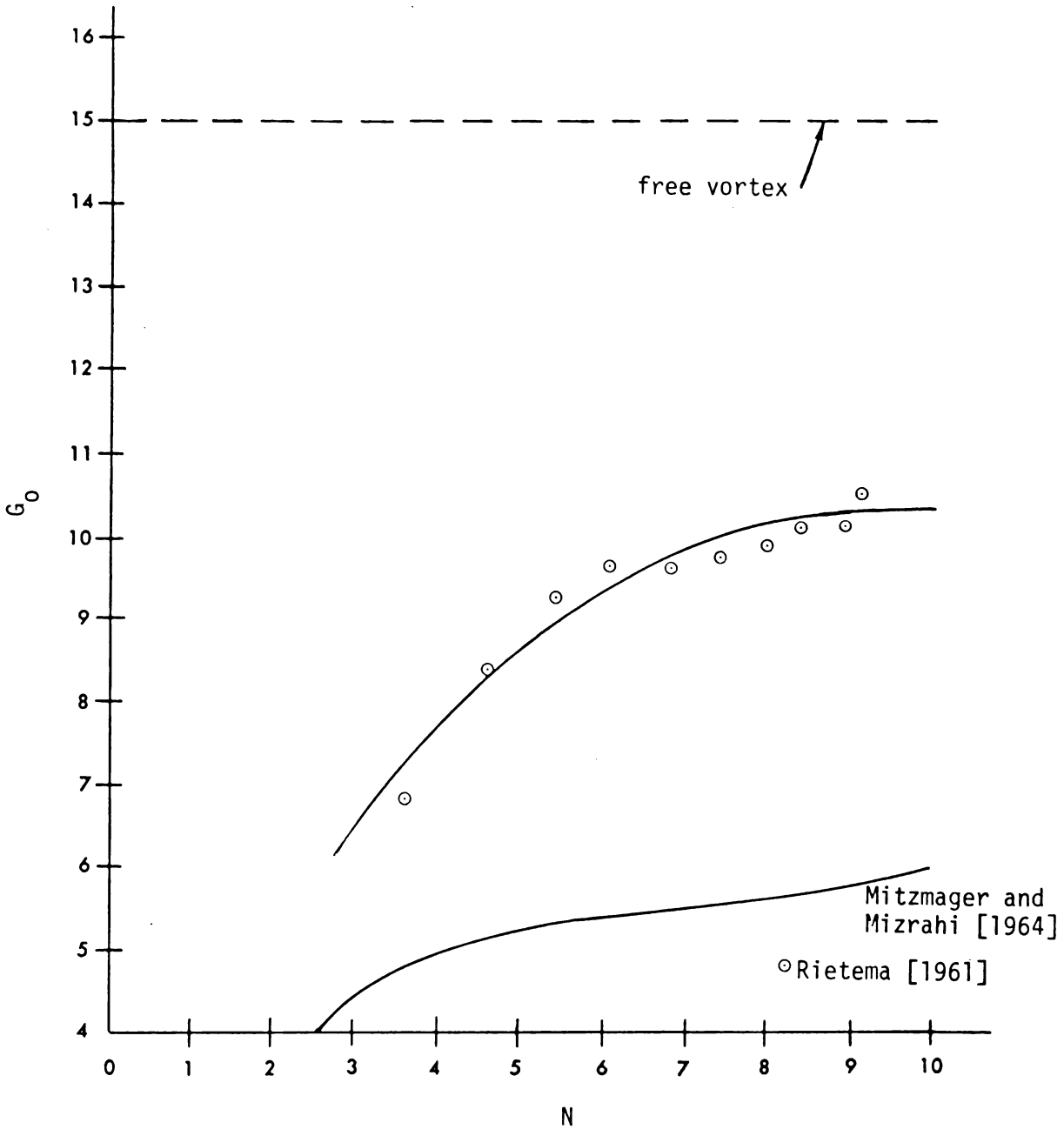

Figure 5.2. The effect of Reynolds number on the pressure loss factor for a single 10mm hydrocyclone (water, 25°C).

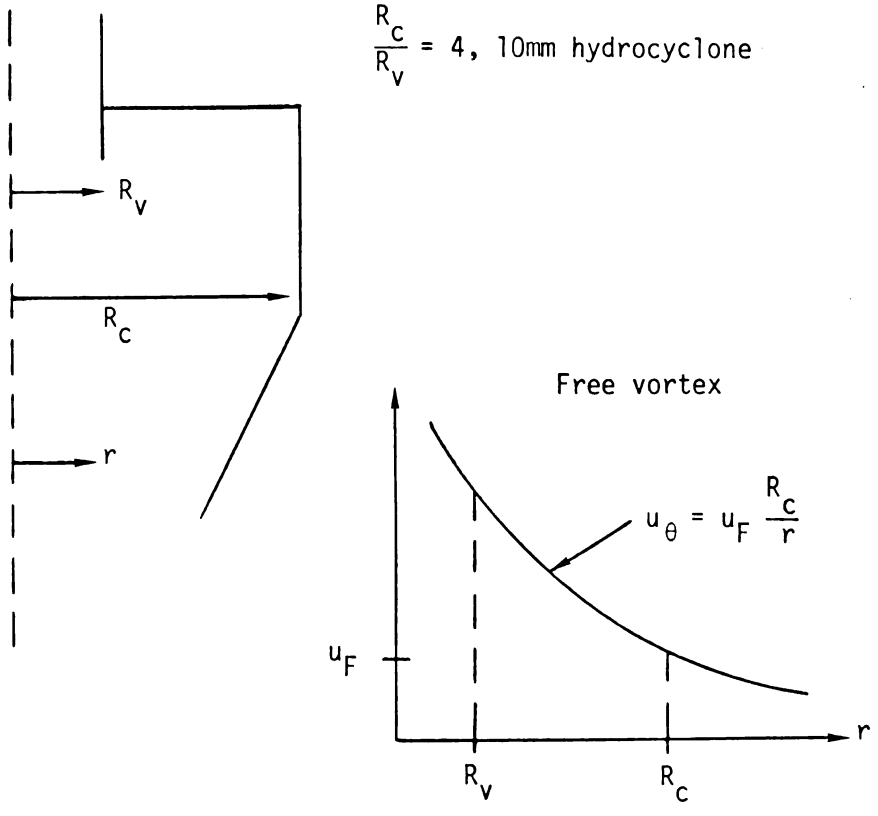

$$\frac{dp}{dr} = \frac{\rho u_\theta^2}{r} \Rightarrow$$

$$\frac{P_c - P_v}{\frac{1}{2}\rho U_F^2} = \left(\frac{R_c}{R_v}\right)^2 - 1$$

Figure 5.3. Free vortex model for pressure loss coefficient.

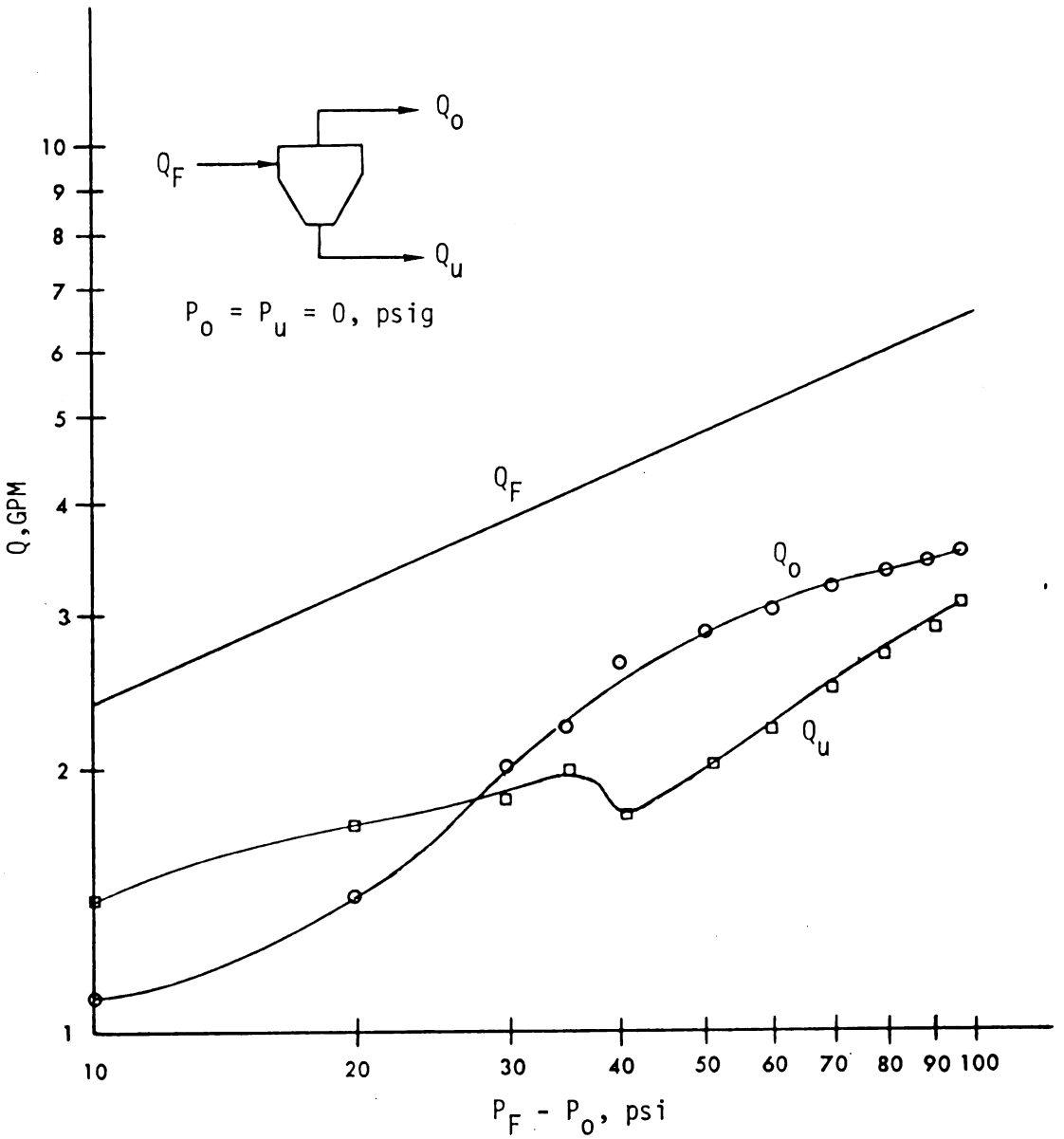

Figure 5.4. The effect of pressure drop on the underflow and overflow rates of six 10mm hydrocyclones (water, 25°C).

cluster of hydrocyclones studied here, some unexpected features were observed, especially when a small amount of polymer is added to the feed stream (see Section 5.2). Note that Q_u suddenly decreases for $P_F - P_o \simeq 35$ psi and then increases again but at a faster rate. For $P_F - P_o < 20$ psi, the overflow and underflow streams are very small (trickles) so the desired flow patterns inside the hydrocyclones may not occur.

Figure 5.5 shows the split ratio Qo/Qu as a function of Reynolds number and should be compared with our previous discussion in Section 2.1.2. Dorr-Oliver reports that the "natural" split for this hydrocyclone is 1.5, which is close to the maximum observed in Figure 5.5.

Although the overflow and underflow discharge freely, the backpressures within the vortex finder and the apex discharge may not be balanced. This may explain the unusual behavior shown in Figure 5.5. An explanation of the dependence of Qo/Qu on Re_F could possibly be developed by using flow visualization; however, in what follows we try to develop some additional insight by applying backpressure to the discharge streams.

Figure 5.6 shows how the addition of backpressure to overflow and underflow streams flattens the split ratio curve. The value observed is 0.77 which is significantly lower than the natural split reported by Dorr-Oliver of 1.5. Constricting the overflow and underflow streams may shift the resistance to flow from the internal manifolds (see Figure 3.2) to the external valves.

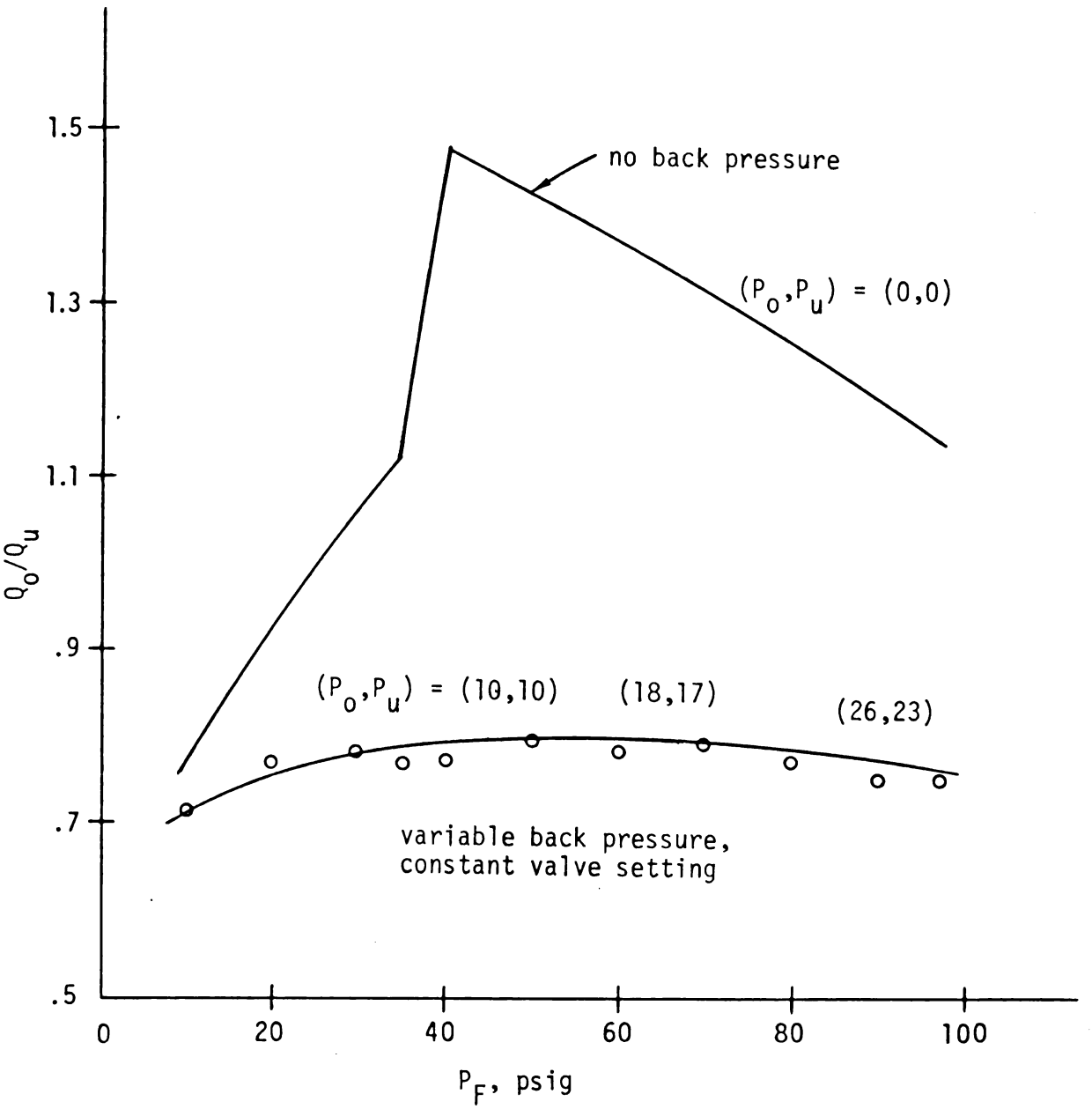

Figure 5.6. The effect of back pressure on the split ratio (water, 25°C).

Table 5.1 shows various results for the effect of backpressure on the capacity, split ratio, and pressure loss coefficient for both polymer and water. Unequal backpressure (Po ≠ Pu) is also investigated. Experiments 1, 2 and 10, 11 indicate that the overflow offers less resistance to flow due to its lower loss coefficient Gu (see Notation). Additionally, the loss coefficient is increased with the addition of polymer (see also, Figure 5.9).

Table 5.2 shows how an increase in viscosity (due to a decrease in temperature) decreases the loss factor G_o and decreases the split ratio. This is an important result and it agrees with the literature results discussed in Section 2.1.2. Additionally, it helps support the fact that the polymer is affecting flow structures inside the hydrocyclone in a manner not associated with the viscosity changes.

5.2 Flow Characteristics With Polymer Additives

The flow characteristics of the 10mm hydrocyclone can be altered significantly by the addition of only 100 wppm polymer. These changes cannot be accounted for by the change in viscosity alone. Thus the polymer is affecting the mechanisms inside the hydrocyclone in an unknown manner.

Figure 5.7 shows the reduction in total capacity associated with the addition of polymer. Others (see Section 2.1.1) have reported that the hydrocyclone capacity increases with viscosity. Because the addition of polymer increases the viscosity and correspondingly decreases the capacity, the polymer

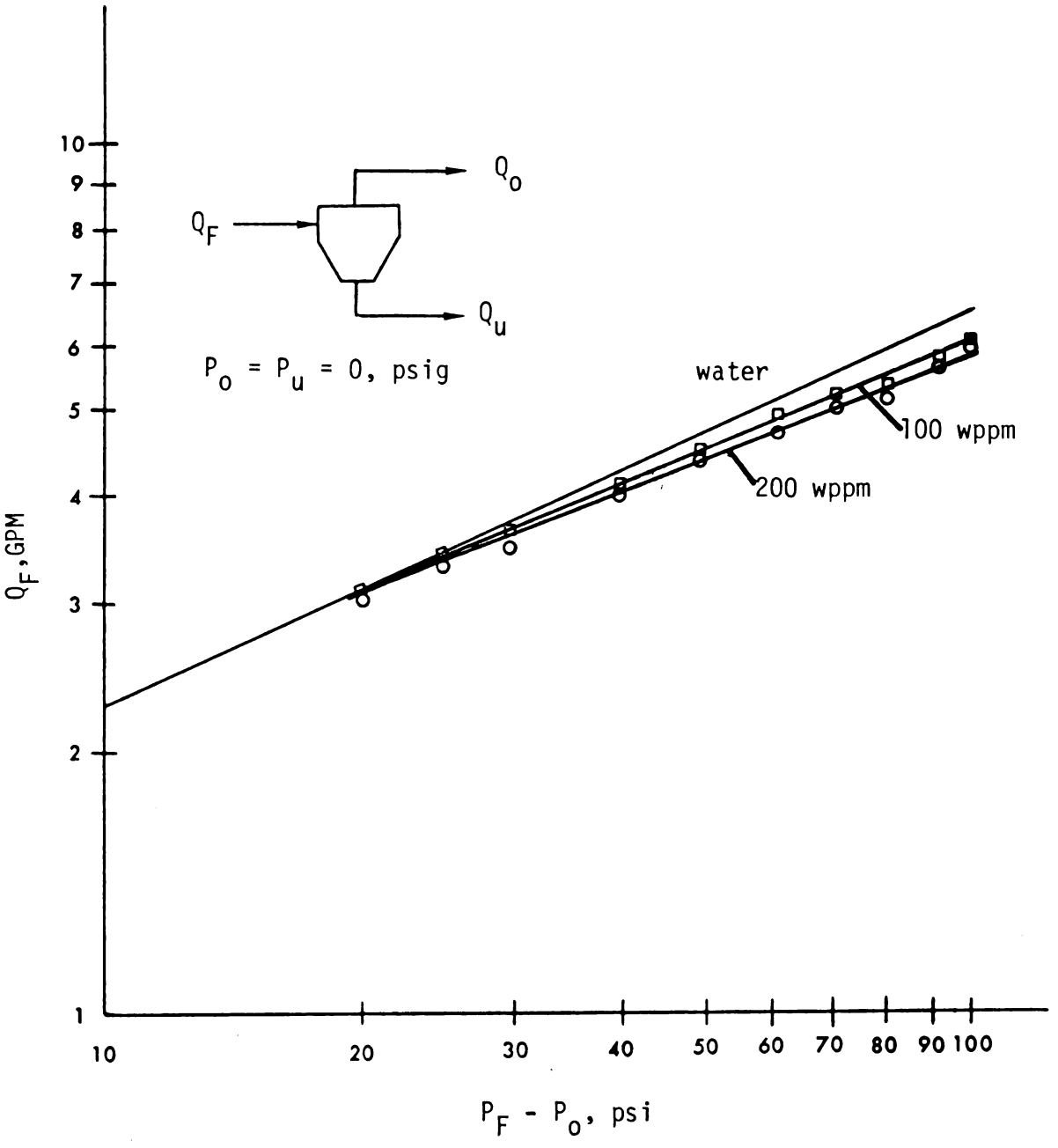

Figure 5.7. The effect of polymer on the capacity of six 10mm hydrocyclones (AP-30, 25°C).

TABLE 5.1.--The Effect of Backpressure on the Capacity and Pressure Loss Coefficients (Water, 1-11; 100 wppm AP-30, 12-16).

Exp	Pressure, psig P_F	P_o	P_u	$Re_F \times 10^{-4}$	G_o	G_u	Qo/Qu
1	70	0	-	3.32	10.96	-	∞
2	70	-	0	3.16	-	12.07	0
3	70	0	0	3.50	9.87	9.87	1.264
4	70	10	0	3.35	9.22	10.76	0.22
5	70	0	10	3.24	11.54	9.89	4.03
6	25	0	0	2.20	8.90	8.90	0.967
7	35	10	10	2.14	9.39	9.39	0.766
8	25	2.5	0	2.21	7.95	8.83	0.40
9	25	0	1	2.19	8.65	8.30	3.27
10	25	0	-	2.22	8.73	-	∞
11	25	-	0	2.13	-	9.48	0
12	70	0	-	3.01	13.31	-	∞
13	70	-	0	3.09	-	12.63	0
14	70	0	0	2.89	11.73	11.73	1.65
15	70	10	0	2.82	10.58	12.34	0.23
16	70	0	10	2.73	13.11	11.24	6.79

TABLE 5.2.--The Effect of Viscosity on the Capacity and Loss Coefficient (water).

T°C	μ, cp	$P_F - P_o$, psi	$Re_F \times 10^{-4}$	G_o	Qo/Qu
16.5	1.105	10	1.30	6.79	0.757
25	0.900	10	1.59	6.84	0.760
16.5	1.105	40	2.24	9.16	1.19
25	0.900	40	2.68	9.63	1.46
16.5	1.105	90	3.21	10.02	1.13
25	0.900	90	3.92	10.11	1.16
16.5	1.105	60	2.71	9.37	1.17
25	0.900	60	3.26	9.75	1.35

is suspected of altering the tangential velocity fields found in the hydrocyclone. Furthermore, if the solution viscosity is increased by merely lowering the water temperature, a resultant increase in capacity is observed.

The addition of polymer also increases the pressure loss factor G_o as seen in Figure 5.8. This indicates that the polymer solution requires a higher pressure drop to obtain the same kinetic energy in the feed stream. Additionally, the polymer solution is also closer to the free vortex value for G_o.

Figure 5.9 shows the increase in the split ratio curve due to the polymer. This is consistent with results obtained by Wallace [1980] but inconsistent with the results of others discussed in Section 2.1.2. Primarily, the increase in the split ratio was due to a corresponding decrease in the underflow rate. The change in mechanism observed for the water case at a feed pressure of ~35 psig is enhanced by the polymer. Chiou and Gordon [1976] have observed that the tangential and axial velocities in a draining tank are reduced by the addition of a small amount of polymer. Since the qualitative velocity profiles in a hydrocyclone are similar to those in a draining tank, this may be a possible explanation for the decrease in the underflow rate.

Figures 5.10 and 5.11 show the alteration in the split ratio for two polymer concentrations at a constant feed pressure. The results for 100 and 200 wppm are almost identical except at the feed pressure closest to the change in mechanism observed in Figure 5.9.

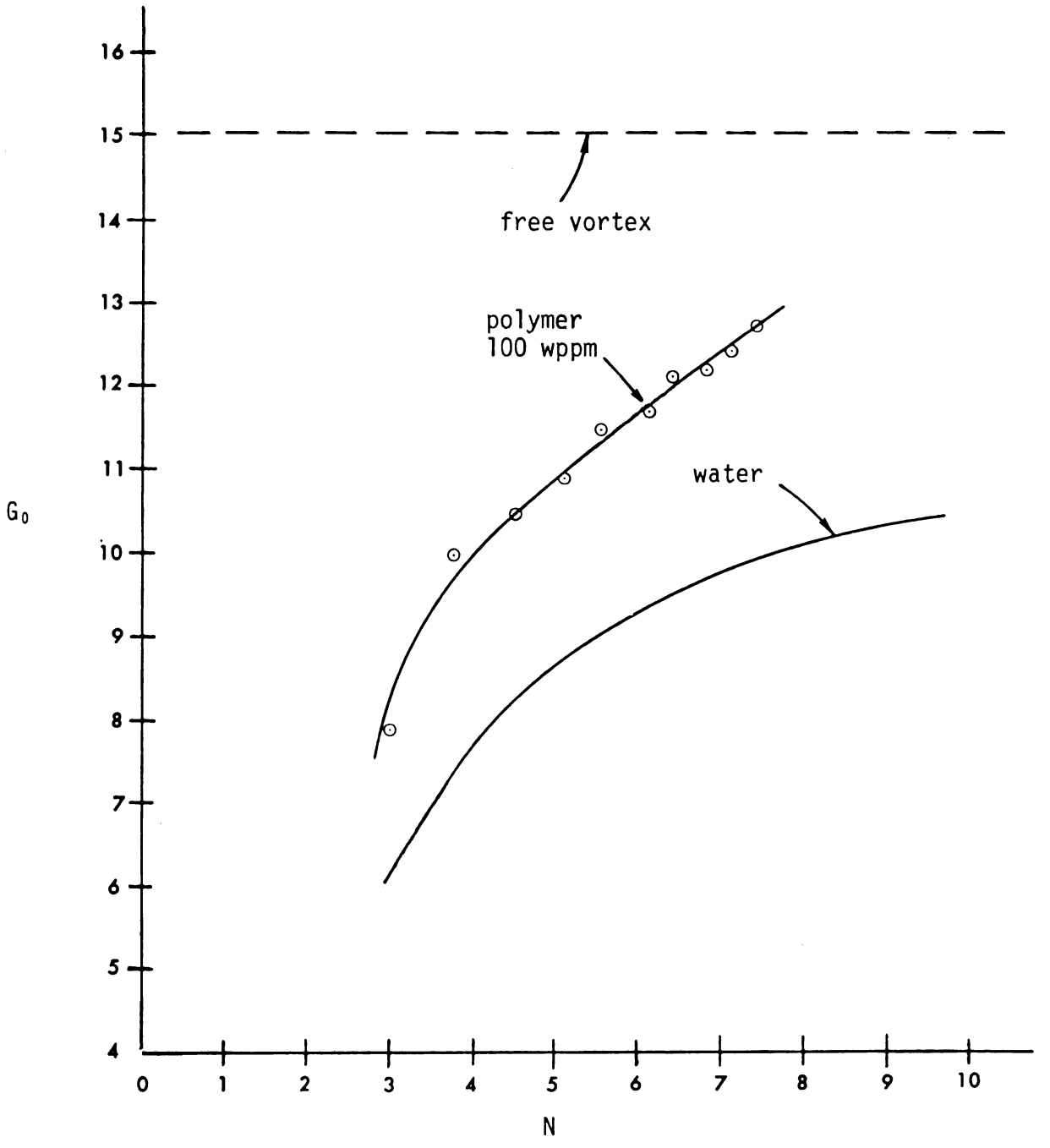

Figure 5.8. The effect of polymer on the pressure loss factor for a single 10mm hydrocyclone (100 wppm AP-30, 25°C).

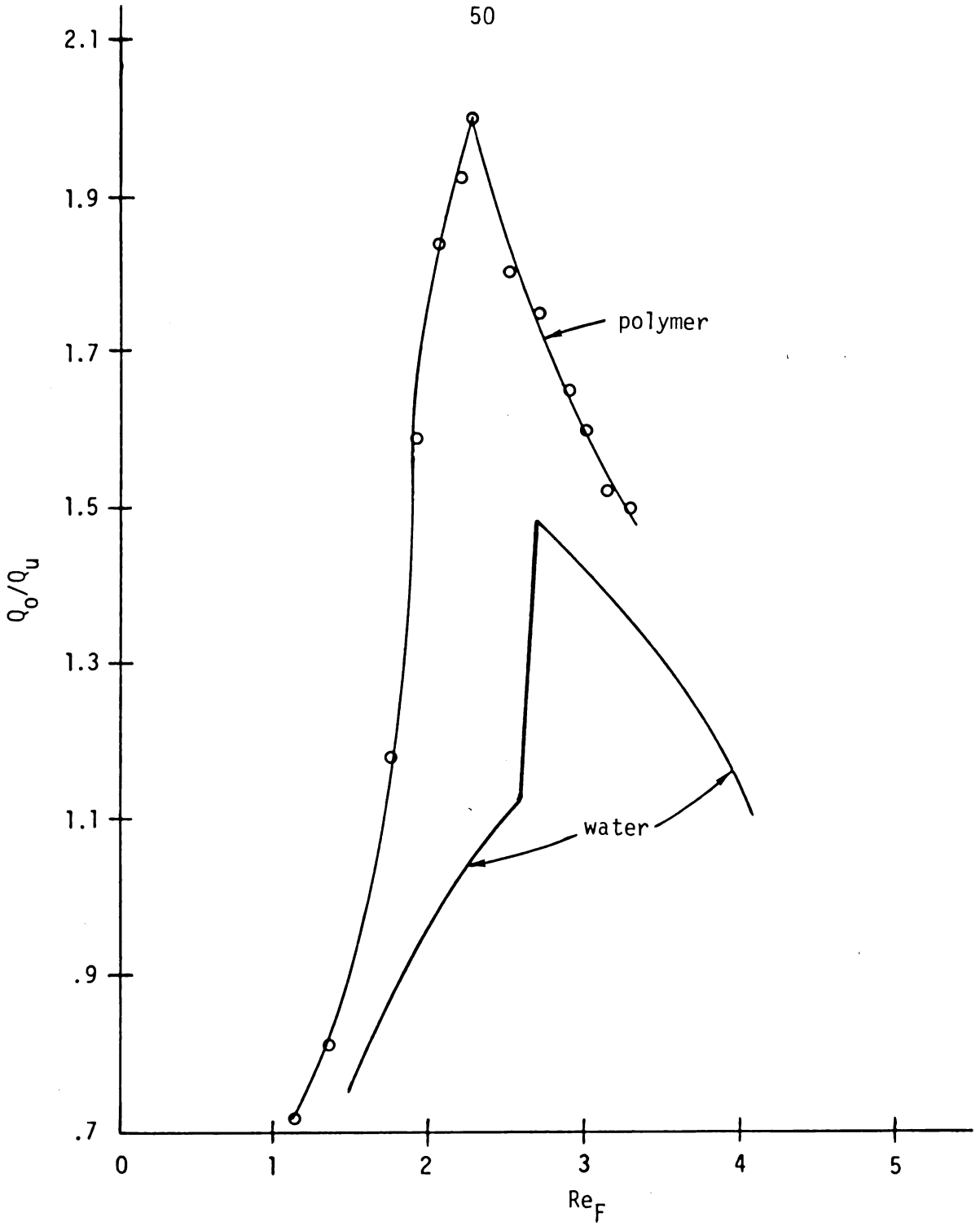

Figure 5.9. The effect of polymer on the split ratio (100 wppm AP-30, 25°C).

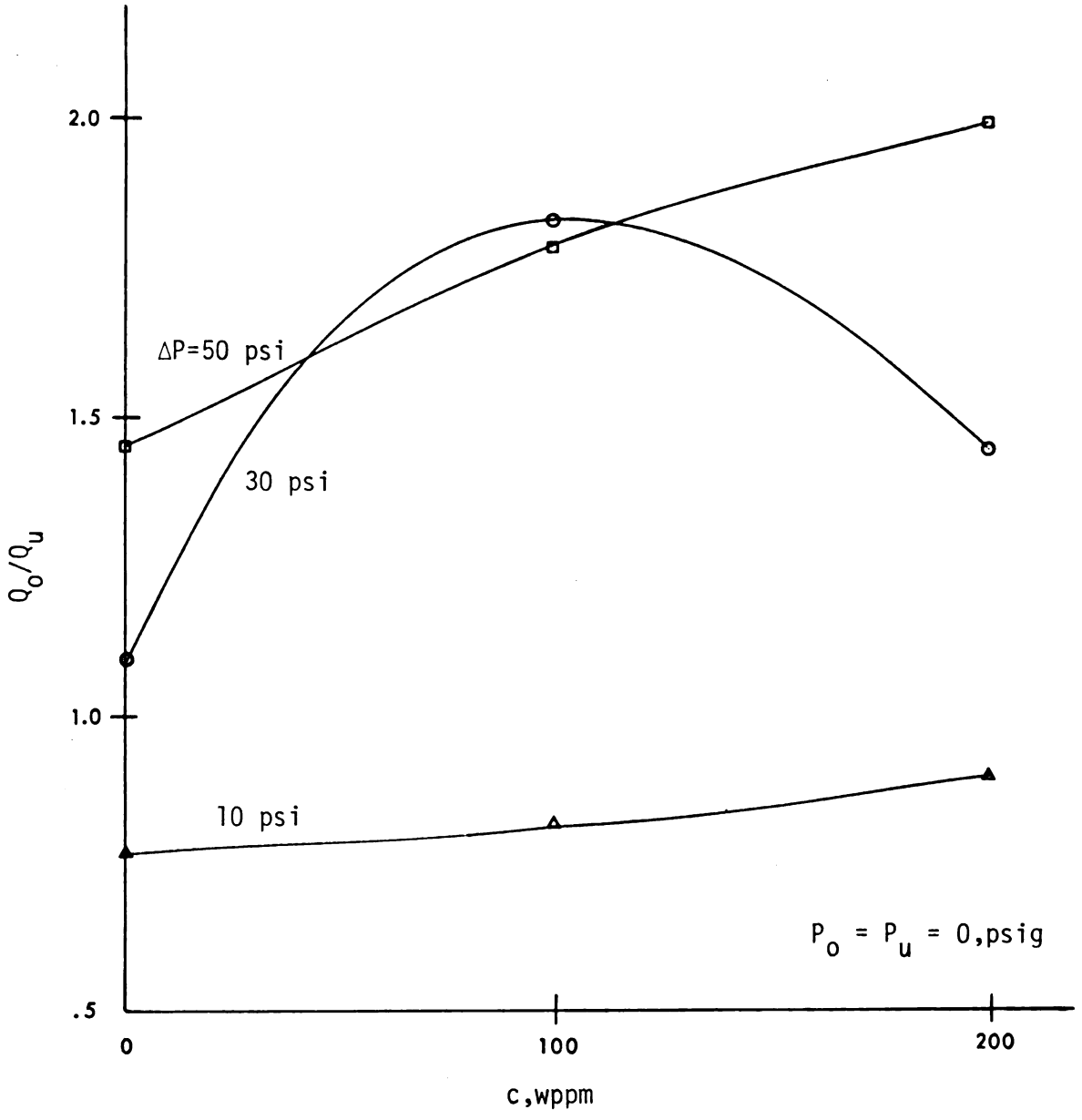

Figure 5.10. The effect of polymer concentration on the split ratio for $\Delta P \leq 50$ psi.

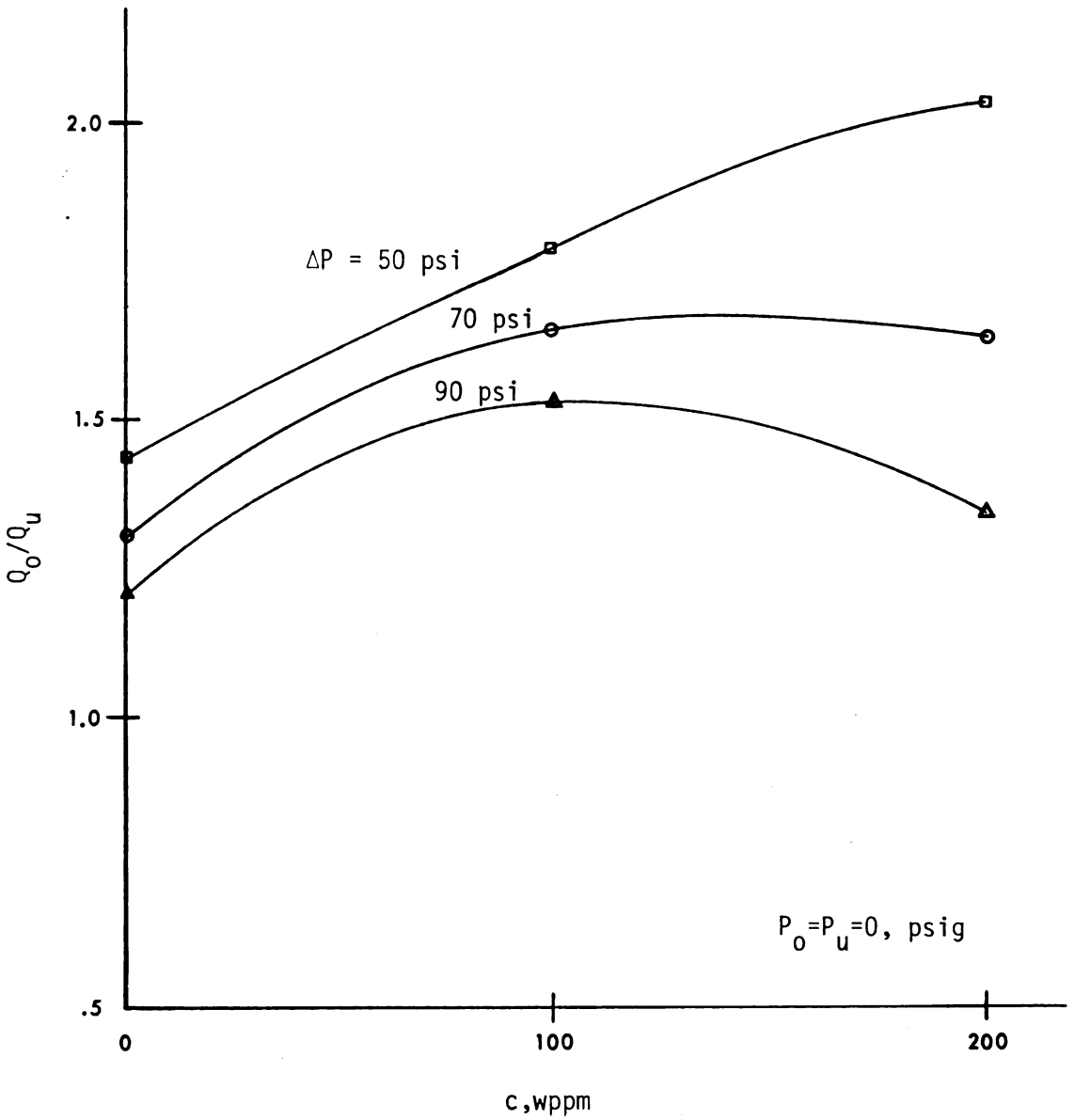

Figure 5.11. The effect of polymer concentration on the split ratio for $\Delta P \geq 50$ psi.

Figure 5.12 shows the effect of flow history on the split ratio. The arrows indicate the direction in which data were recorded by starting with fresh polymer solutions. Because it takes approximately 20 minutes to record data for a complete run, the % drag reduction differs for the two curves at the ends but not in the middle. It is believed that this accounts for the differences in the observed split ratio values. Differences in the split ratio for water were not observed when the order of recording the data was reversed.

The transient behavior of the split ratio due to the polymer is observed in Figure 5.13. The result for mixing strategy I and II and the no clay case are qualitatively the same, except the clay case has a higher asymptote. Note that none of the solutions obtain a value of 2.0 observed in Figure 5.9. The critical time frame is the first 5 minutes after the polymer is added. During this time not only is the split ratio changing very rapidly but, as shown in the next section, the highest values of centrifugal efficiency are observed.

5.3 Separation Characteristics With and Without Polymer Additives

Another way to indirectly measure changes in the internal flow structures of a hydrocyclone due to polymer addition is to observe the effects it has on centrifugal separation efficiency (see Equation 2.1). While specific changes in the flow structure cannot be identified, changes can be inferred if no other effects are present.

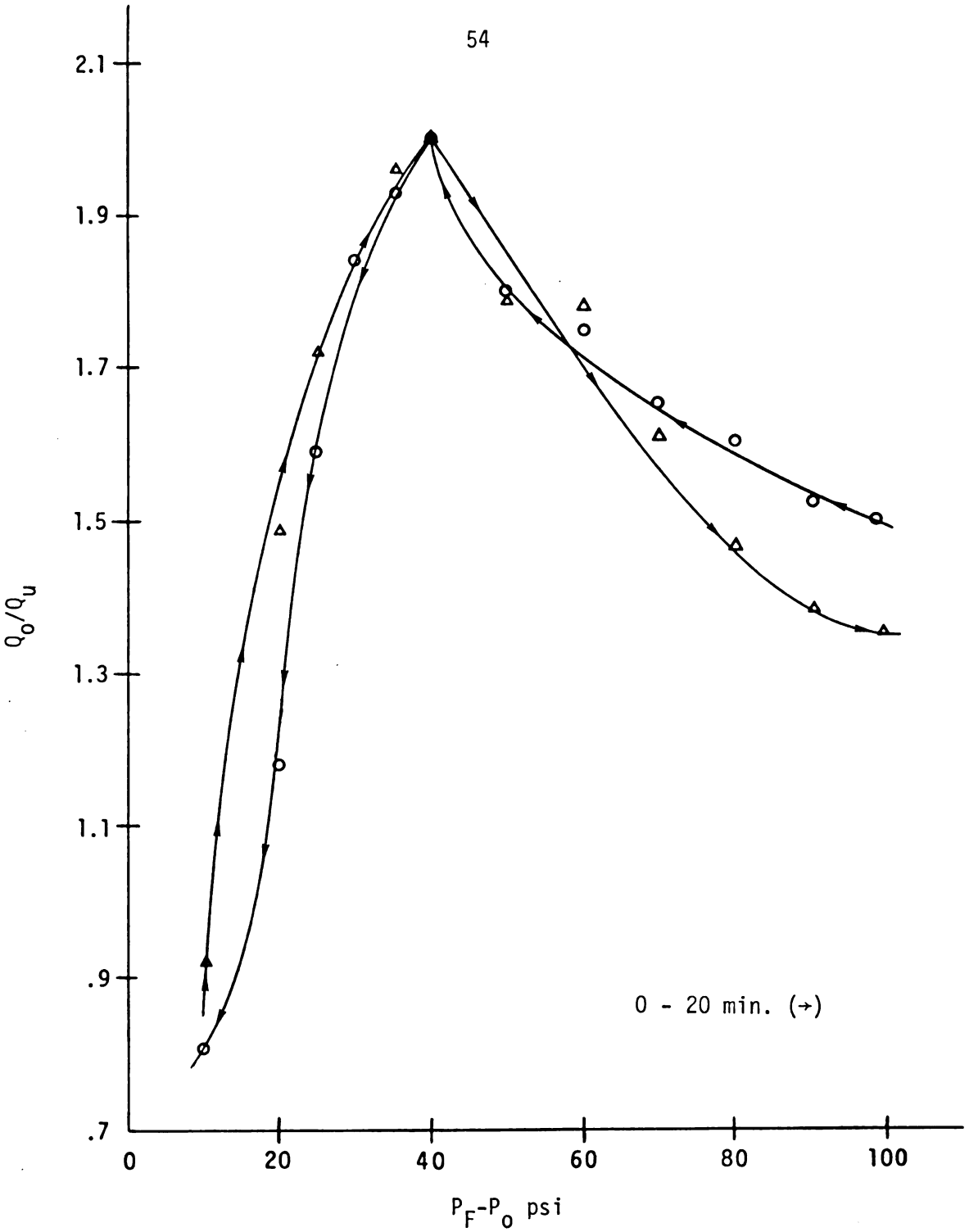

Figure 5.12. The effect of flow history on the split ratio (100 wppm AP-30, 25°C).

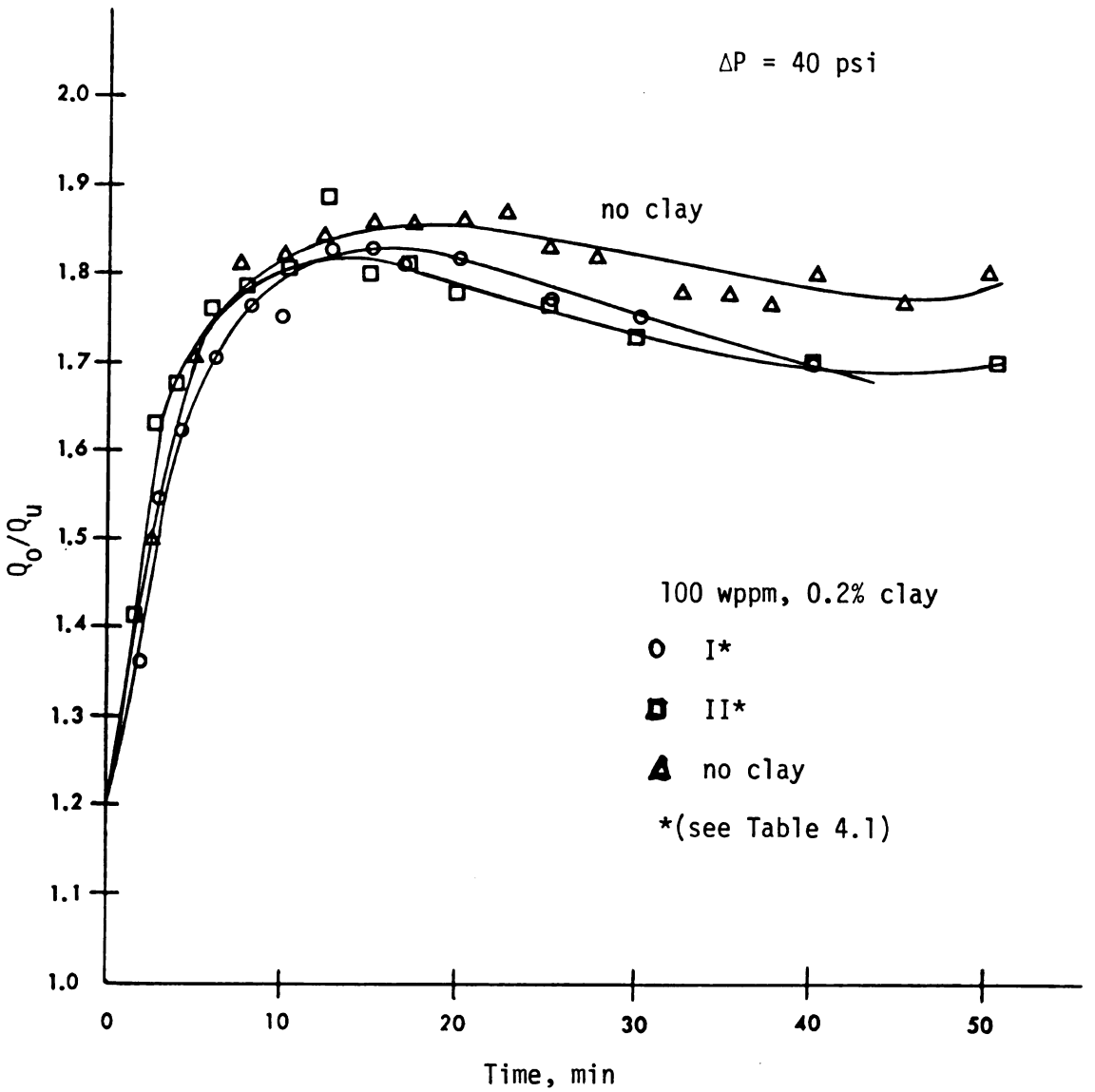

Figure 5.13. The effect of mixing strategy on the split ratio at ΔP = 40 psi (25°C).

Figure 5.14 shows the effect of polymer concentration and Reynolds number on the centrifugal efficiency for mixing strategy I. The increase in the efficiency is probably due to two different mechanisms. First, the polymer reduces the swirl velocity, as mentioned in Section 5.2, and thus the centrifugal force felt by the clay particles. Second, the effective particle diameter is increased due to flocculation of the polymer and clay as discussed in Section 2.2. These 'flocs,' however, are easily destroyed and thus the change in diameter is small - possibly only 4 or 5 clay particles combined. Additionally, the time frame of the transient observed is 5-10 minutes which corresponds to the transients observed for the split ratio in Section 5.2 and the drag reduction in Appendix A.

A 200 wppm solution yields a separation efficiency which is below the 100 wppm solution because it further reduces the swirl velocity but has little effect on the flocculation. It should be noted that no flocculation was observed during any of the runs by visual inspection. However, changing the effective diameter from 1μ to 5μ is not an effect that would be apparent.

The Reynolds number also has an effect on the centrifugal efficiency. For both the polymer cases and the no polymer case an increase in the Reynolds number produced a corresponding increase in the efficiency. This is consistent with results reported by Haas, et al. [1957] and others in the literature (see Section 2.1.3).

Figure 5.15 shows that the transient behavior observed (A) can be eliminated by altering the polymer mixing strategy. By

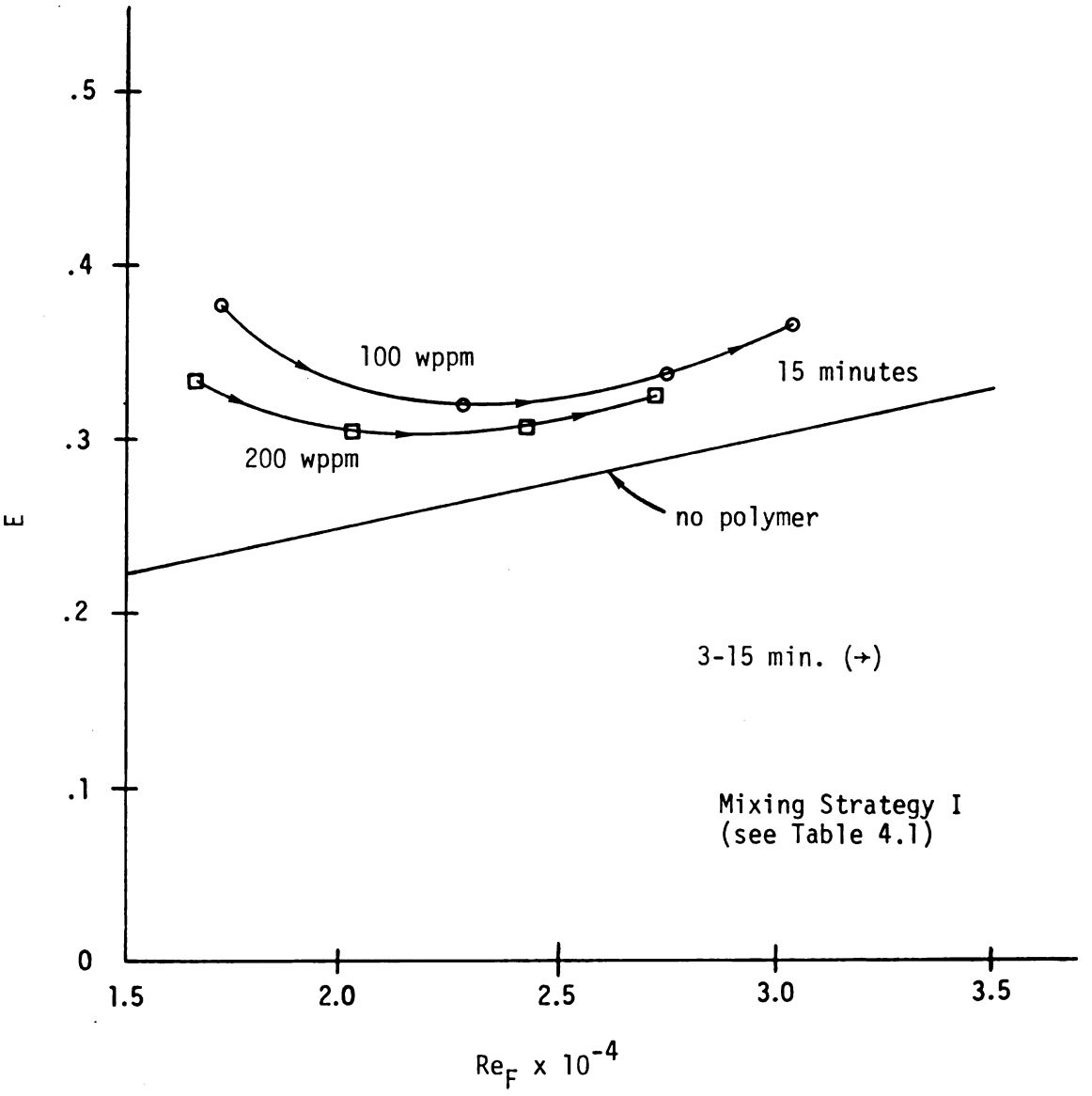

Figure 5.14. The effect of Reynolds number and polymer concentration on the centrifugal efficiency for a 10mm hydrocyclone (0.2 wt% clay, 25°C).

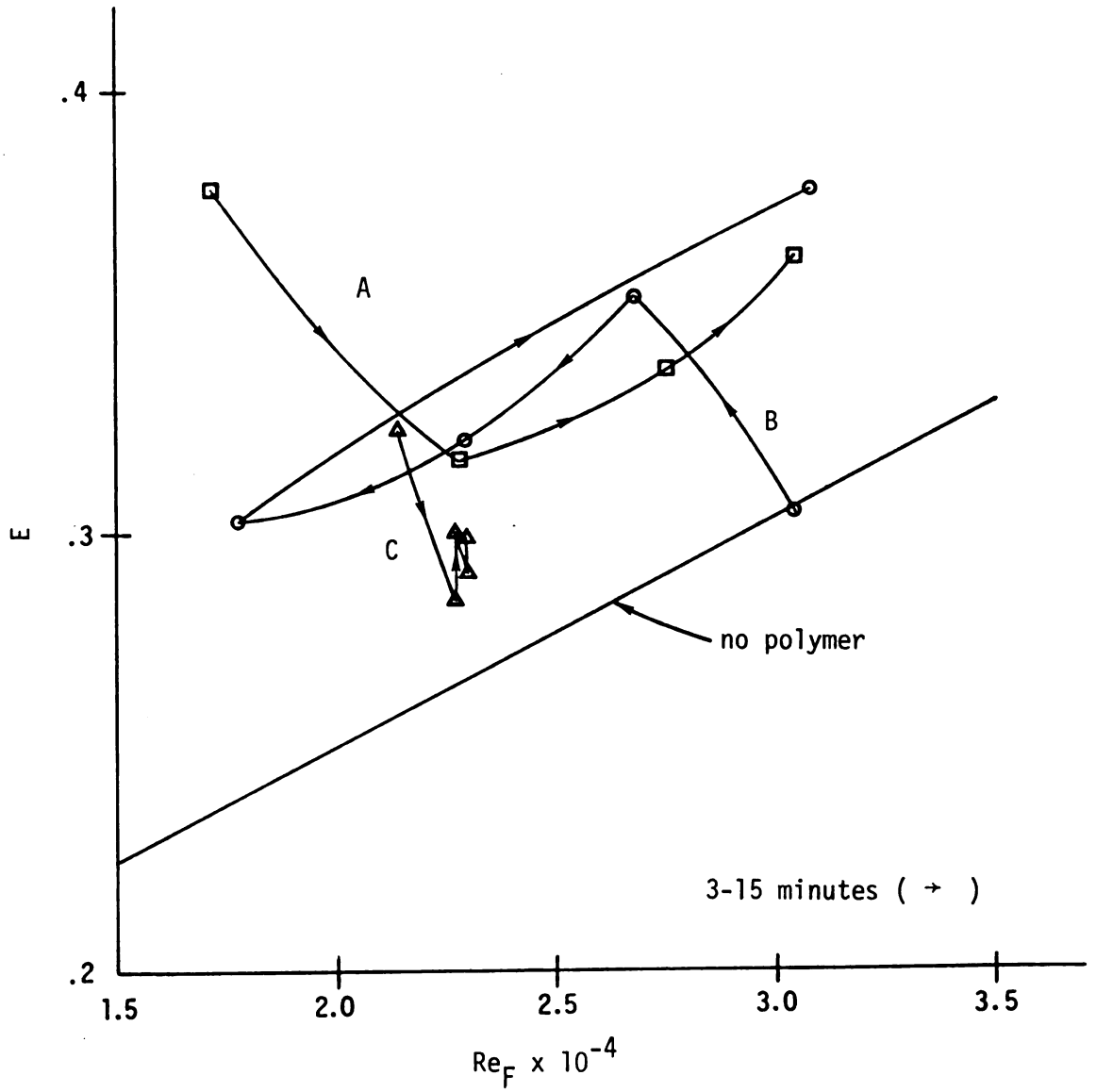

Figure 5.15. The effect of polymer history on the centrifugal efficiency of a 10mm hydrocyclone (0.2 wt% clay, 100 ppm AP-30, 25°C; A: Flow loop mixing of polymer; B: Gentle turbine mixing of polymer; C: Hand mixing of polymer, clay added wet).

gently shearing the polymer with a turbine on a low speed setting (B) or hand mixing (C) the transients are greatly reduced. The efficiency for B has a higher asymptote than the flow loop mixing for A.

Polymer degradation can also reduce transient behavior as shown in Figure 5.16. Preparation B has been degraded for 30 minutes by the pumps yet it yields the highest efficiency data reported and has no transient behavior. The addition of 100 wppm polymer to B brings it below the no polymer case as shown by C. Presumably, this additional polymer slows the swirl velocity yet does not help flocculate the clay.

Figure 5.17 compares the results for mixing strategies I and II. When the polomer is added first (I), the centrifugal efficiency shows a significant increase over the no polymer and clay first (II) cases. The 200 wppm cases are both below their corresponding 100 wppm cases which supports the lowering of the swirl velocity argument in Section 5.2. This anomolous effect was first observed by Wallace [1980].

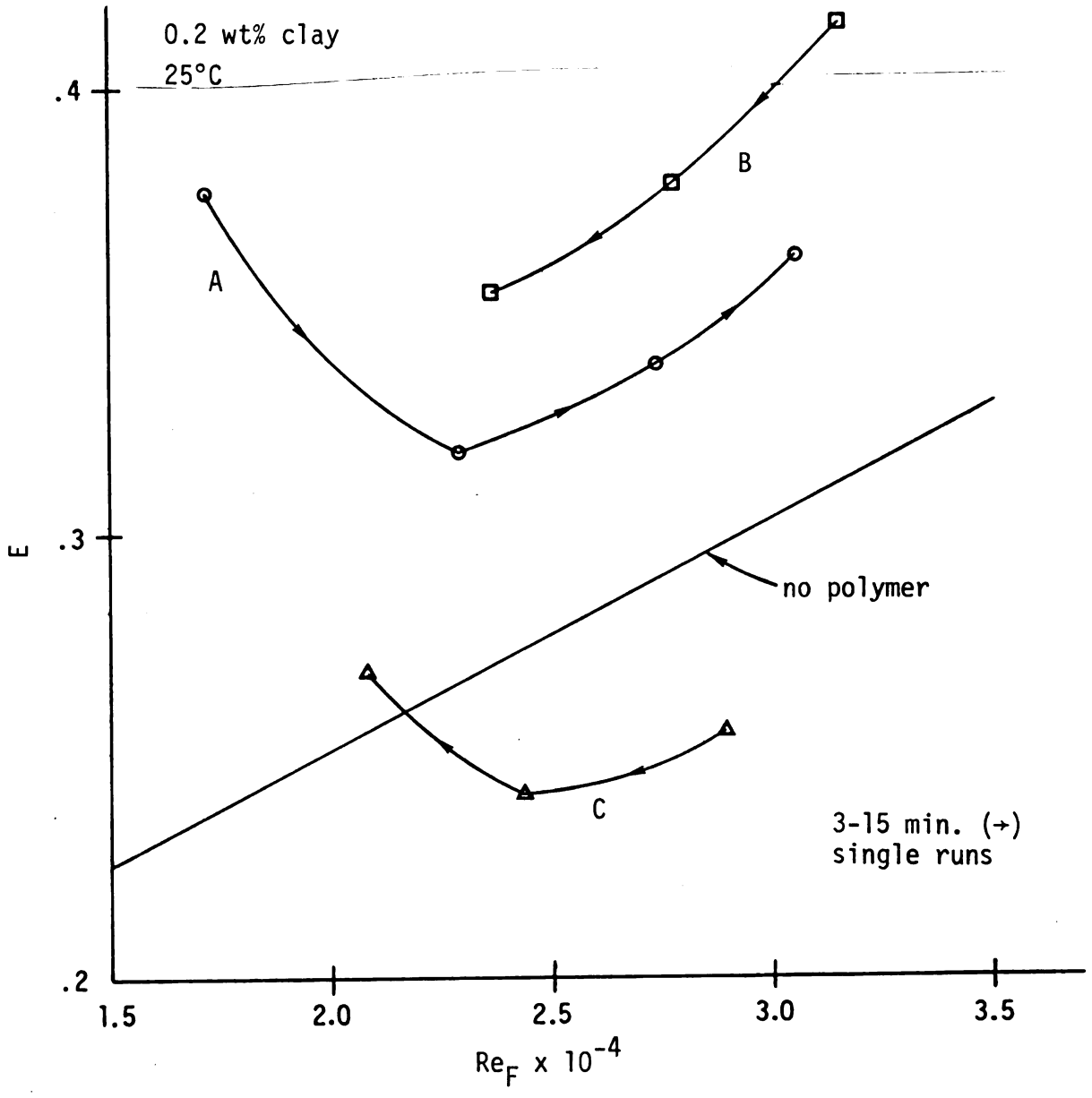

Figure 5.16. The effect of severe polymer degradation on the centrifugal efficiency of a 10mm hydrocyclone (A: 100 wppm polymer, 0.2 wt% clay, flow loop mixing, 65% initial drag reduction; B: 100 wppm polymer, flow loop mixing for 30 minutes, 25% initial drag reduction; C: 200 wppm polymer prepared by adding dry polymer to B).

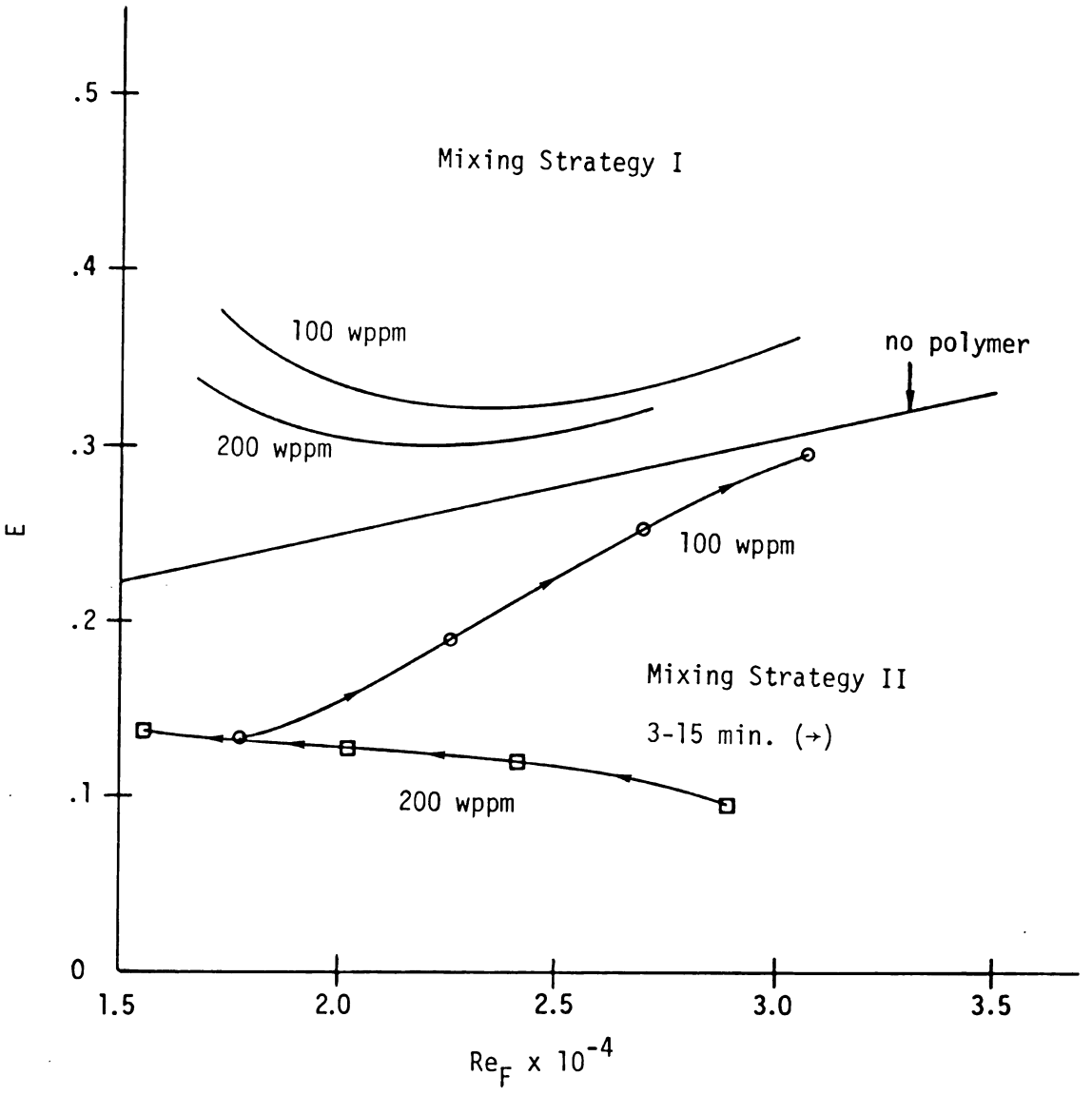

Figure 5.17. The effect of mixing strategy II on the centrifugal efficiency of a 10mm hydrocyclone (0.2 wt% clay, 25°C).

CHAPTER 6

CONCLUSIONS AND RECOMMENDATIONS

The addition of Separan AP-30 to the feed stream of a 10mm hydrocyclone seems to have altered some important internal flow structures. In particular, one of the flow structures which controls the underflow stream has been weakened. The reduction in the underflow stream can be observed in Figure 5.9. This data possibly suggests a decrease in the swirl velocity and, more importantly, the centrifugal forces similar to that observed by Chiou and Gordon [1976]. This reduction hypothesis is consistent with the results obtained for the separation experiments portrayed in Figure 5.17. Although the addition of polymer to the solution increases the viscosity slightly, this has an opposite effect on hydrocyclone performance than simply increasing the viscosity by lowering the temperature. This conclusion follows by comparing the pressure loss coefficient, G_o, for the polymer solution (see Table 5.1) and water at 25°C and 16°C (see Table 5.2). Thus, the polymer alters flow structures within the hydrocyclone which are unaffected by comparable changes in viscosity.

The mixing strategy paradox (see Chapter 1) was determined to be dependent on the order in which the polymer-clay-water suspension was mixed and not to any "pre-stretching" of the polymer (cf.

Wallace, 1980). The differences in efficiency for mixing strategies I and II were believed to be due to polymer-clay flocculation (see Section 2.3), although no evidence of this flocculation was observed directly. However, the amount of flocculation required for the observed changes in efficiency would be minimal and quite possibly unobservable. The reason why mixing strategy I should promote flocculation relative to II remains unclear.

It is noteworthy that both mixing strategies yield polymer-clay-water suspensions which exhibit similar drag reducing characteristics for fully developed pipe flow (see Figure A.3). Moreover, the two different mixing strategies showed no important differences in the capacity and the split ratio of the hydrocyclone, although these differed significantly from the no polymer studies. Thus our main conclusion based on a set of indirect observations is that, in the absence of flocculation, the addition of Separan AP-30 to the feed stream reduces the centrifugal efficiency (lower curve in Figure 5.17). For clay suspension this adverse effect can be compensated by particle flocculation, provided the clay and polymer are mixed according to strategy I (see Table 4.1). This yields the upper curve in Figure 5.17.

Obviously, further research in this area should include an investigation into the flocculating capabilities of Separan AP-30 with kaolinite clay. Other high molecular weight polymers, which have a greater or lesser tendency to flocculate with clay, should be investigated. Two excellent choices would be the copolymers which make up Separan AP-30, polyacrylamide and polyacrylate.

It is already known that they affect flow structures in turbulent pipe flow (Virk, 1975) and thus are good candidates to affect flow structures in hydrocyclones. Flow visualization should also be considered in order to determine exactly which flow fields are being altered by the polymer. This may lead to a better understanding of how hydrocyclones operate and thus improve and expand their applications.

APPENDICES

APPENDIX A

VISCOSITY AND FRICTION FACTOR MEASUREMENTS

APPENDIX A

VISCOSITY AND FRICTION FACTOR MEASUREMENTS

A.1 Apparatus

The flow characteristics of the various mixtures used in the hydrocyclone experiments (see Table 4.1) were determined for a straight capillary tube in parallel with the Doxie 5 Dorrclone (see Figure 3.1). The specific design parameters for the capillary are listed in Table A.1.

The inside diameter of the tube was measured by inserting a drill bit into the cut ends of the tube and measuring its diameter with a micrometer. Visual inspection of the tube ends showed no crimping. The design gave an entrance length of 250 D so a fully developed profile in the test section would occur. Both monometers produced steady readings for all the measurements reported. Accurate low Reynolds number measurements were difficult for clay suspensions with more than 0.2 wt % solids.

A.2 Procedure and Results for Viscosity Measurements

Apparent viscosities of the polymer-water-clay suspensions used in the hydrocyclone studies were measured by applying the Hagen-Poiseuille equation for fully developed laminar flow of a Newtonian fluid in a circular tube. By measuring the volumetric

flow rate Q and the pressure drop ΔP (>0), the viscosity was calculated as follows

$$\mu = \frac{\pi R^4}{8L} \quad \frac{\Delta P}{Q} \tag{A.1}$$

where R and L represent, respectively, the radius and length of the tube (see Table A.1). Flow rates were measured by timing and weighing the fluid exiting the capillary tube; the pressure drop was measured manometrically.

The hydrostatic equation for the manometer and Equation (A.1) can be combined to give a final working equation for the viscosity in terms of the mass flow rate W and the change in height of the manometer fluid ΔH. The result is

$$\mu = K \frac{\Delta H}{W} \tag{A.2}$$

where

$$K \equiv \frac{\pi R^4}{8L} \quad \rho^2 g \left(\frac{\rho_{CC\ell_4}}{\rho} - 1\right). \tag{A.3}$$

With the units of μ in cp, ΔH_c in inches of $CC\ell_4$, and W in ℓbm/sec, Equation (A.2) becomes

$$\boxed{\mu = 6.767 \times 10^{-4} \quad \frac{\Delta H_c}{W}} \; . \tag{A.4}$$

All of the mixtures used in this study (see Table 4.) showed the behavior

$$W \propto \Delta H_c \tag{A.5}$$

for low flow rates. Therefore, Equation (A.4) was used to define the viscosities experimentally. A typical set of experimental data is shown in Appendix B and the final results for the viscosities are tabulated in Table A.2. The pH of each solution was measured using pH paper but only varied from 7.0 to 7.3 for all the systems studied.

TABLE A.1.--Design Parameters for Capillary Tube.

Material:	drawn steel (carbon)
Inside diameter:	0.146" (3.708 mm)
Length between pressure taps:	89" (2.26m)
Entrance length:	36" (0.914m)
Pressure taps:	Branch welded
U-tube manometers:	$cc\ell_4$ for low Re Hg for high Re

Although the viscosities listed in Table A.2 are not significantly different from the solvent (H_2O), these values were used whenever a characteristic Reynolds number was calculated (see, for example, the results presented in Section 5.3). Earlier Wallace [1980] assumed that the viscosity of the dilute polymer solutions at high shear rates would be equal to the solvent viscosity. This idea was not tested in this study and should be investigated further. It is noteworthy, however, that the maximum strain rate in the capillary tube at Re = 10^3 is approximately 800 sec^{-1} for water. Therefore, the apparent shear viscosities for the dilute polymer

TABLE A.2.--Viscosities Measured Using the Small Capillary Tube.

T,°c	Concentration wppm Polymer	Clay	Mixing strategy (see Table 4.)	μ,cp
25	0	0		0.909(.8904)*
↓	100	↓	-	1.001
	200			1.001
	300			1.201
25	0	100	-	0.895
↓	↓	2000		0.981
25	100	100	I	1.024
	200			1.149
↓	300	↓	↓	1.260
25	100	2000	I	1.004
↓	↓	↓	II	1.0045
15°	0	0	-	1.158(1.139)*
↓	100	0	-	1.195
	100	100	I	1.200

*CRC, 1981

solutions listed in Table A.2 may be appropriate for correlating data obtained in the hydrocyclone experiments.

Applications of Equation (A.1) assumes that the fluid is effectively Newtonian and that the Reynolds number, defined by

$$Re \equiv \frac{2W}{\pi R\mu} , \qquad (A.6)$$

is less than 2100. Obviously, the mass flow rate W, the radius of the tube R, and the viscosity μ all have consistent units in (A.6).

Pressure drop-flow rate data for fully developed flows are often correlated in terms of a friction factor and a Reynolds number given by Equation (A.6). The Fanning friction factor, defined by

$$f \equiv \tau_w / \tfrac{1}{2}\rho u_b^2 \ , \tag{A.7}$$

is used here to correlate the flow data in the laminar and turbulent regimes. In Equation (A.7), τ_w is the average wall shear stress and u_b is the bulk average velocity. Because both ends of the capillary tube are at the same height, an overall force balance on the fluid in the tube is

$$2\pi RL\tau_w = \pi R^2 \Delta P. \tag{A.8}$$

Equation (A.8) holds for all Reynolds numbers (laminar or turbulent flows) and for all fluids (Newtonian and non-Newtonian). Eliminating τ_w between (A.7) and (A.8) gives an expression for f in terms of the observable pressure drop and flow rate, viz.,

$$f = \frac{R}{2L} \frac{\Delta P}{\tfrac{1}{2}\rho u_b^2} \cdot \tag{A.9}$$

Introducing the mass flow rate,

$$W \equiv \rho u_b \pi R^2 \ , \tag{A.10}$$

and the hydrostatic equation for the manometer into Equation (A.9) given

$$f = \left(\frac{\pi^2 R^5 \rho g(\rho_m - \rho)}{L} \right) \frac{\Delta H}{W^2} \cdot \tag{A.11}$$

The densities of the mixtures studied were assumed to be the same and equal to 62.31 $\ell bm/ft^3$. Thus, a final working equation for the friction factor used in this work is

$$f = \begin{cases} 1.476 \times 10^{-6} \dfrac{\Delta H_m}{W^2}, & \text{mercury} \\ 6.969 \times 10^{-8} \dfrac{\Delta H_c}{W^2}, & \text{carbon tetrachloride} \end{cases} \qquad \text{(A.12)}$$

In Equation (A.12), W has units of ℓbm/sec whereas ΔH_m and ΔH_c have units of inches of mercury and carbon tetrachloride, respectively.

For laminar flow, Equation (A.1) is equivalent to

$$f = 16/Re \qquad \text{(A.13)}$$

where f and Re are given by Equations (A.11) and (A.6), respectively. The working equation (A.12) gives f in terms of the measured parameters ΔH_c and W. Figure A.1 shows how f depends on Re for some of the mixtures used in this research. Because μ was determined by Equation (A.4), which is really a rearrangement of Equation (A.13), it should not be surprising that all the data correlate with Equation (A.13); the relevant experimental observation is contained in expression (A.5).

A.3 Procedure and Results for the Drag Reduction Experiment

Drag reduction information was recorded for the following concentrations of clay and polymer:

- No clay with 0, 100, 200 wppm AP-30
- 100 wppm AP-30 with 0, 100, 400, 20,000 wppm clay.

Most of the data were taken at 25°C although some were taken as low as 15°C. The amount of time that the polymer was mechanically degraded inside the pumps before data was recorded was also an

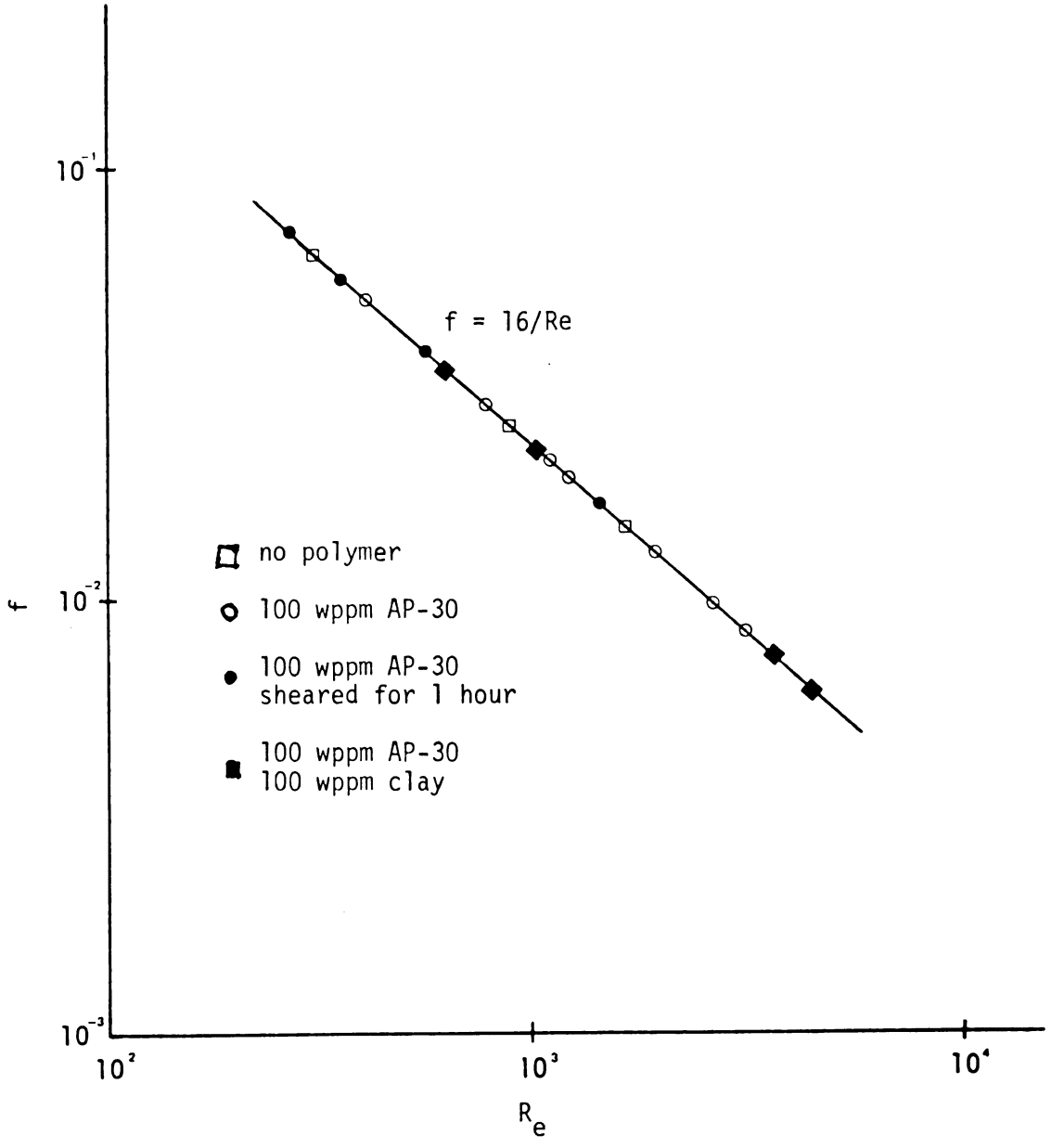

Figure A.1. Friction factor for laminar flow (25°C).

important parameter. This degradation time ranged from 0 to 60 minutes and is shown on each graph in minutes. If no time is mentioned, the shear time is zero and data were taken immediately after mixing the suspension. The order in which the clay and polymer were added to solution was recorded for each run (see Table 4.1). The effect of ageing on the suspension was investigated by allowing a suspension to sit overnight before drag reduction experiments were performed.

To determine the amount of drag reduction present at various polymer and clay concentrations, pressure drop and flow rate data were obtained. The pressure drop across the capillary tube was measured with a water over mercury manometer. The flow rate was measured by allowing the water to flow from the capillary tube into a container where it was weighed and the time was recorded. A typical sample weighed 4.06 ℔bm and took 37.7 seconds. The pressure drop was 45.16 inches of Hg for a Reynolds number of 1.65×10^4 and a friction factor of 6.20×10^{-3} (see Equation (A.12)).

Standard friction factor versus Reynolds number curves for turbulent flow in a pipe were reproduced by measuring pressure drops at various flow rates. A typical set of data is shown in Appendix B. This information was converted to friction factors and Reynolds numbers using Equations (A.6) and (A.12). Viscosity data are recorded in Table A.1. Figure A.2 shows the results for water at 25°C. Although the data fall below the classical Blasius correlation, they are very reproducible. Equation (A.11) shows that the friction factor is very sensitive to the radius of the capillary ($f \propto R^5$).

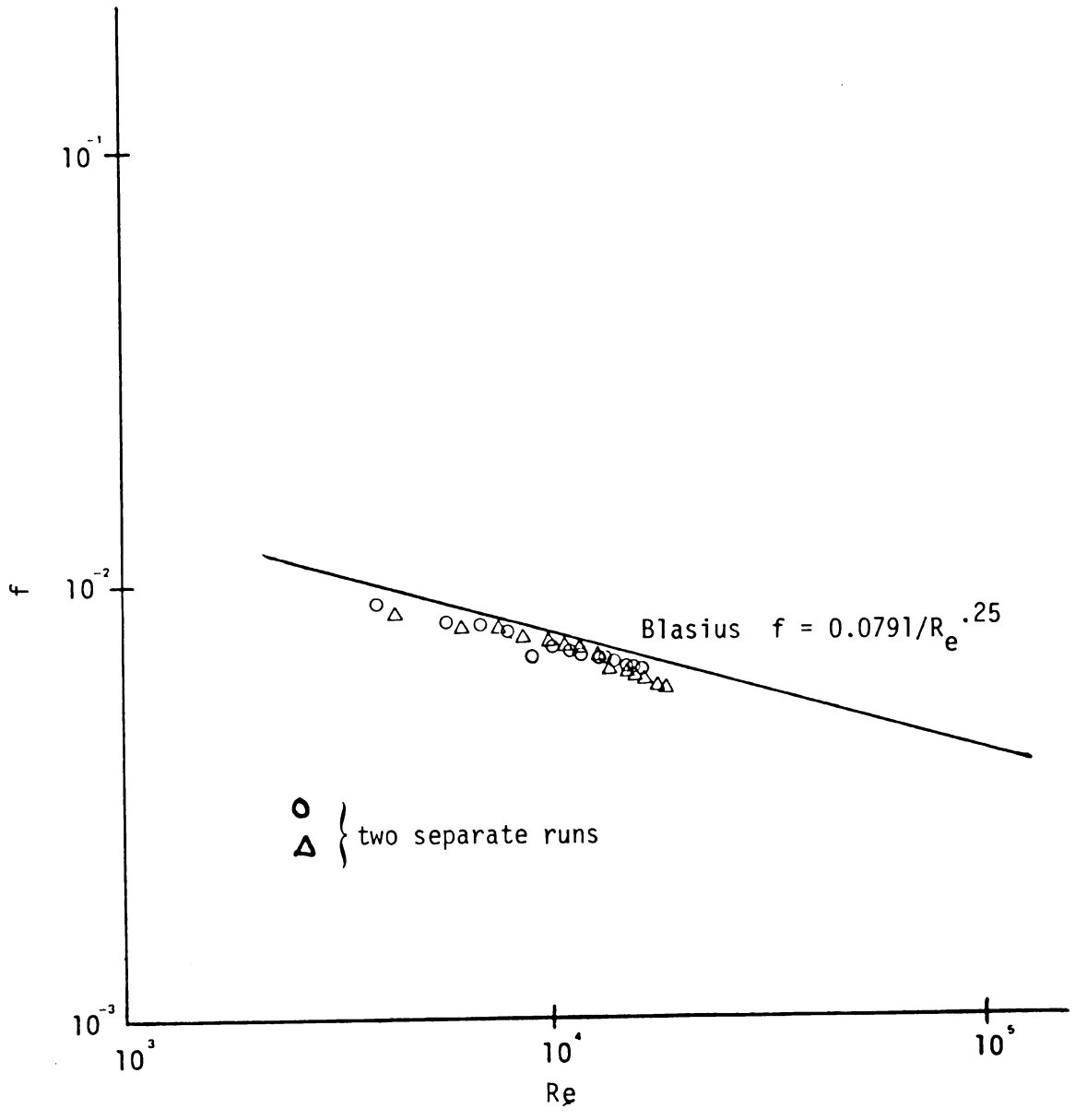

Figure A.2. Friction factor for fully developed turbulent pipe flow (water, 25°C).

An increase of only 1 or 2% in R would move the experimental data onto the Blasius correlation. Also, because $Re \propto 1/\mu$, small errors in the viscosity (see Table A.1) would shift the data in Figure A.2 in the right direction.

Because the polymer seems to degrade significantly during the first hour after preparation, a constant pressure drop experiment was performed to determine the transient behavior of the friction factor for various polymer solutions. Figure A.3, which shows how the mass flow rate changes at constant ΔP, summarizes the main observations made. All of the mixtures tested fell within the hatched area. Within this region small differences between the various runs were observed, but the quantitative significance of this remains unclear. The transient behavior of Mixture E (see legend in Figure A.3) was the largest in magnitude whenever Mixture B was the smallest.

Figure A.3 shows that an initial surge immediately followed the addition of polymer to the system which often made it difficult to stabilize the pressure drop for the first minute or two. Following this initial period, the flow rates dropped from some maximum value, often 50% higher than the flow rate of plain tap water, to a flow rate slightly above that of tap water. Thus, the drag reducing qualities are not completely lost and a residual 10-20% drag reduction effect remains for several hours.

The addition of clay to the suspension has no noticeable effect. Wallace, et al. [1979] and Dabir, et al. [1980] suspected that a small amount of clay might help to stabilize the drag

Mix	Conc. wppm AP-30	Conc. wppm Clay	Prep
A	100	0	--
B	100	100	I
C	100	100	II
D	100	100	I*
E	100	400	II

*Degraded 10 minutes

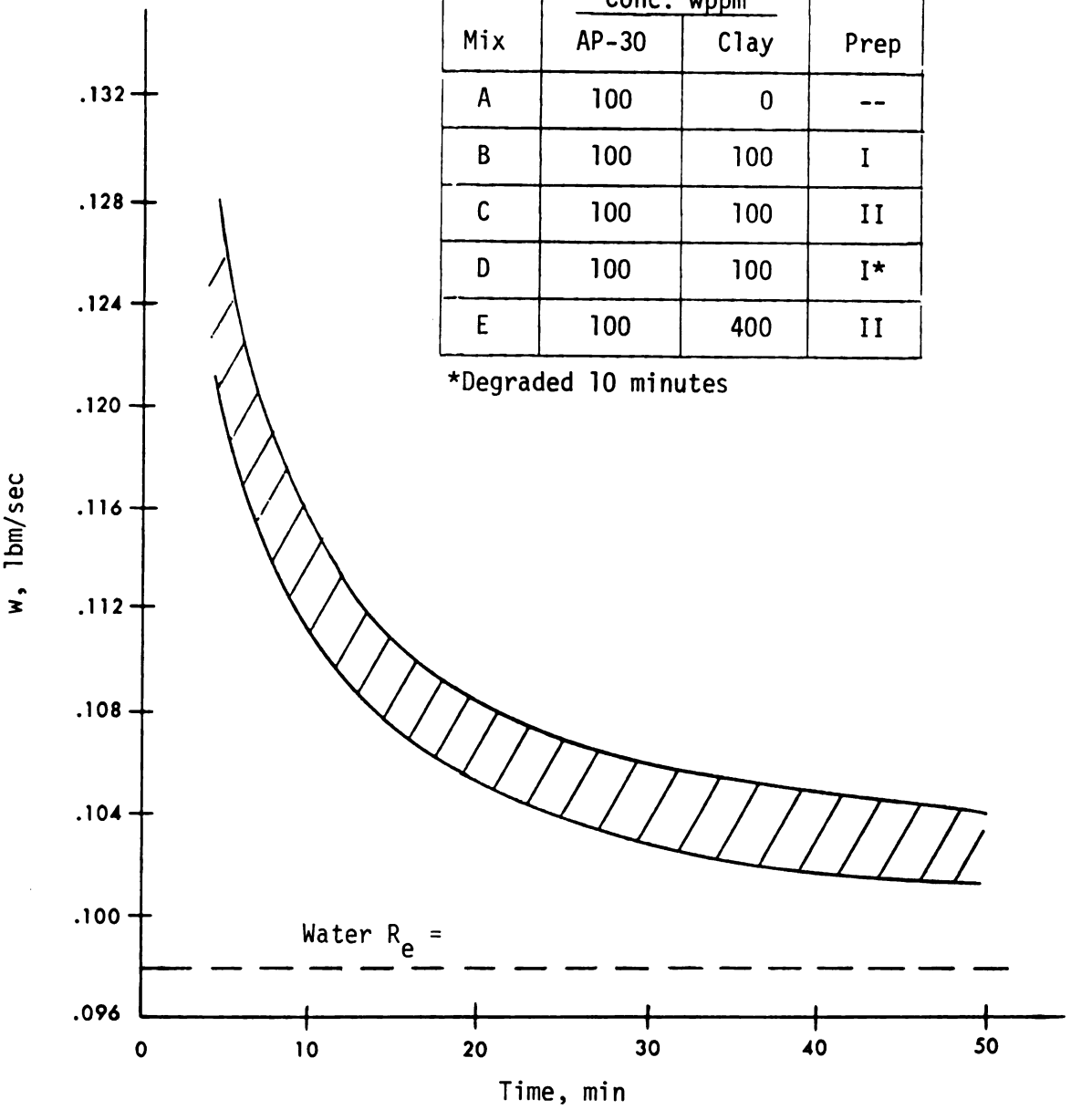

Figure A.3. Transient behavior of various polymer mixtures in turbulent pipe flow (ΔP = 41.63", 25°C).

reducing qualities of the suspension by either retarding polymer degradation or by increasing the residual drag reduction left after mechanical degradation due to the pumps. However, the set of experiments summarized by Figure A.3 does not seem to support this hypothesis.

The transient behavior of five different mixtures fall within the hatched region of Figure A.3. Mixture C is identical in composition to Mixture B but the preparation strategy was reversed (see Table 4.1). No significant differences were noted between Mixtures B and C.

Mixture D was cycled through the pumps for 10 minutes before adding clay. The clay was added to see if this would stop or slow the mechanical degradation. Although the transient decay after the addition of clay remained within the hatched region shown in Figure A.3, there seemed to be a slight reduction in the rate of decay. As mentioned earlier, Mixture E has the highest clay concentration and its transient behavior remained within the hatched region, but was above all the other studies.

Higher concentrations of clay have a dampening effect on the drag reduction. This is shown in Figure A.4 where two different suspensions are compared. Both suspensions contain 100 wppm AP-30 but the clay content of one is 400 wppm whereas the clay concentration of the other is 2%. The 2% clay suspension exhibits drag reduction qualities that are greatly reduced when compared to the 400 wppm suspension. The initial surge that usually accompanies the addition of polymer was very small. Both these suspensions had

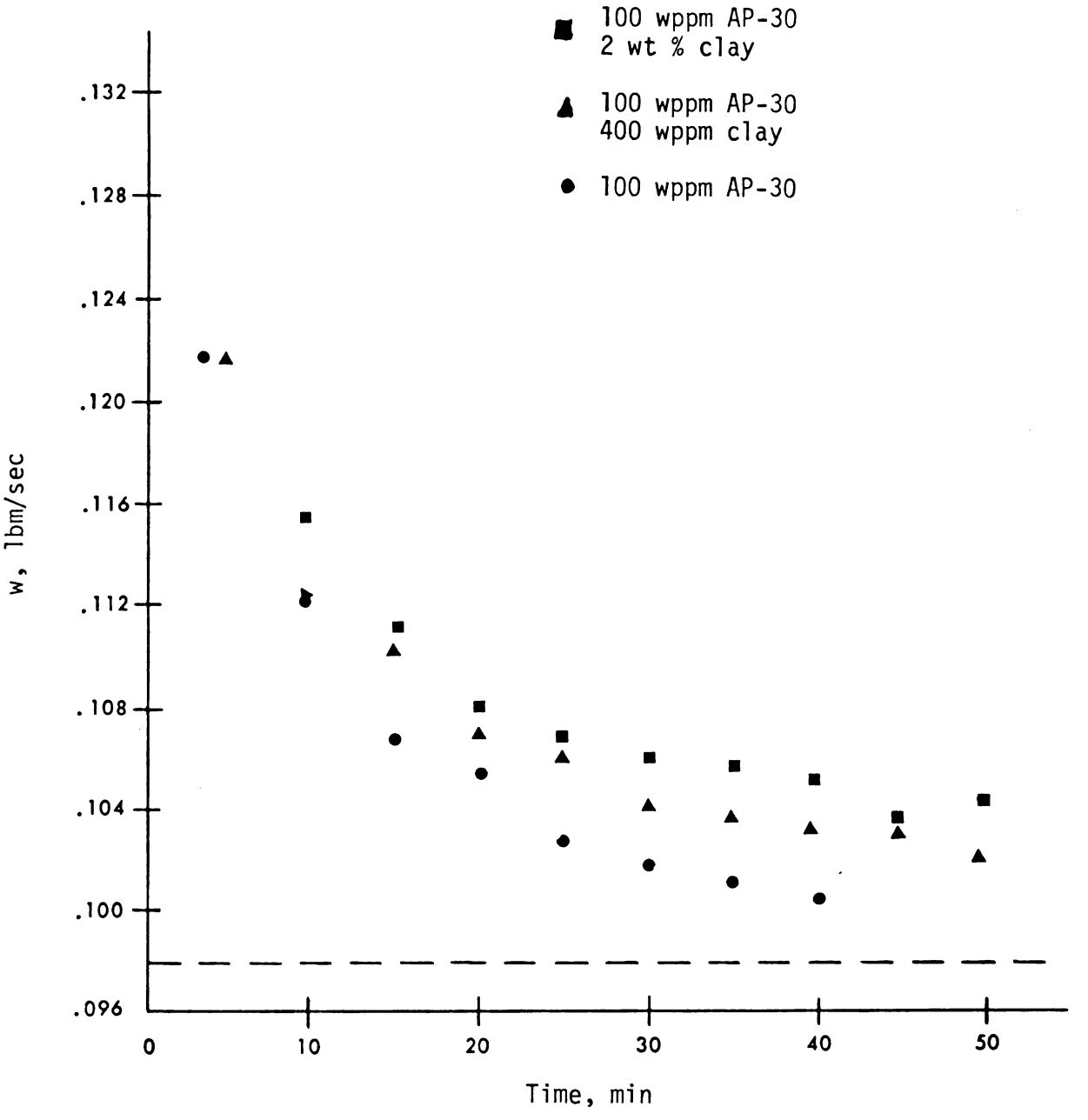

Figure A.4. The effect of clay concentration on polymer degradation in turbulent pipe flow (ΔP = 41.63", 25°C).

the clay added before the polymer. As mentioned in the procedure section, a 2 wt. % solution is difficult to work with due to settling of the clay. This may have caused some problems here due to surging in the capillary tubes and inaccurate flow rate measurements.

The effect of Reynolds number on the drag reduction characteristics of the polymer-clay suspensions used in the hydrocyclone experiments was also determined. Data were recorded from high Reynolds numbers to low Reynolds numbers and took between 1 and 2 hours to complete each run. The amount of time each polymer suspension recycled through the pumps before the experiment started is listed with the graphical results which follow.

In Figure A.5 the first and third cases contain the same polymer concentration but differ in the amount of shearing action. After 30 minutes of recycling through the pumps the 100 wppm AP-30 solution shows little drag reduction. Comparing this to the friction factor data for tap water, only about 10% drag reduction is present. The middle curve is a 200 wppm solution and has been sheared for 60 minutes before taking data. This higher concentration greatly resists the degradation induced by the pumps.

The effect of clay on the drag reducing qualities can be observed in Figure A.6. Here, as before, the data were recorded from high to low Reynolds numbers. In these two runs the exact pressure drops were reproduced so the data could be compared easily. The data show no effect of clay on drag reduction.

The effects of ageing the polymer suspension overnight can be seen in Figure A.7. Both suspensions contain 100 wppm of clay and

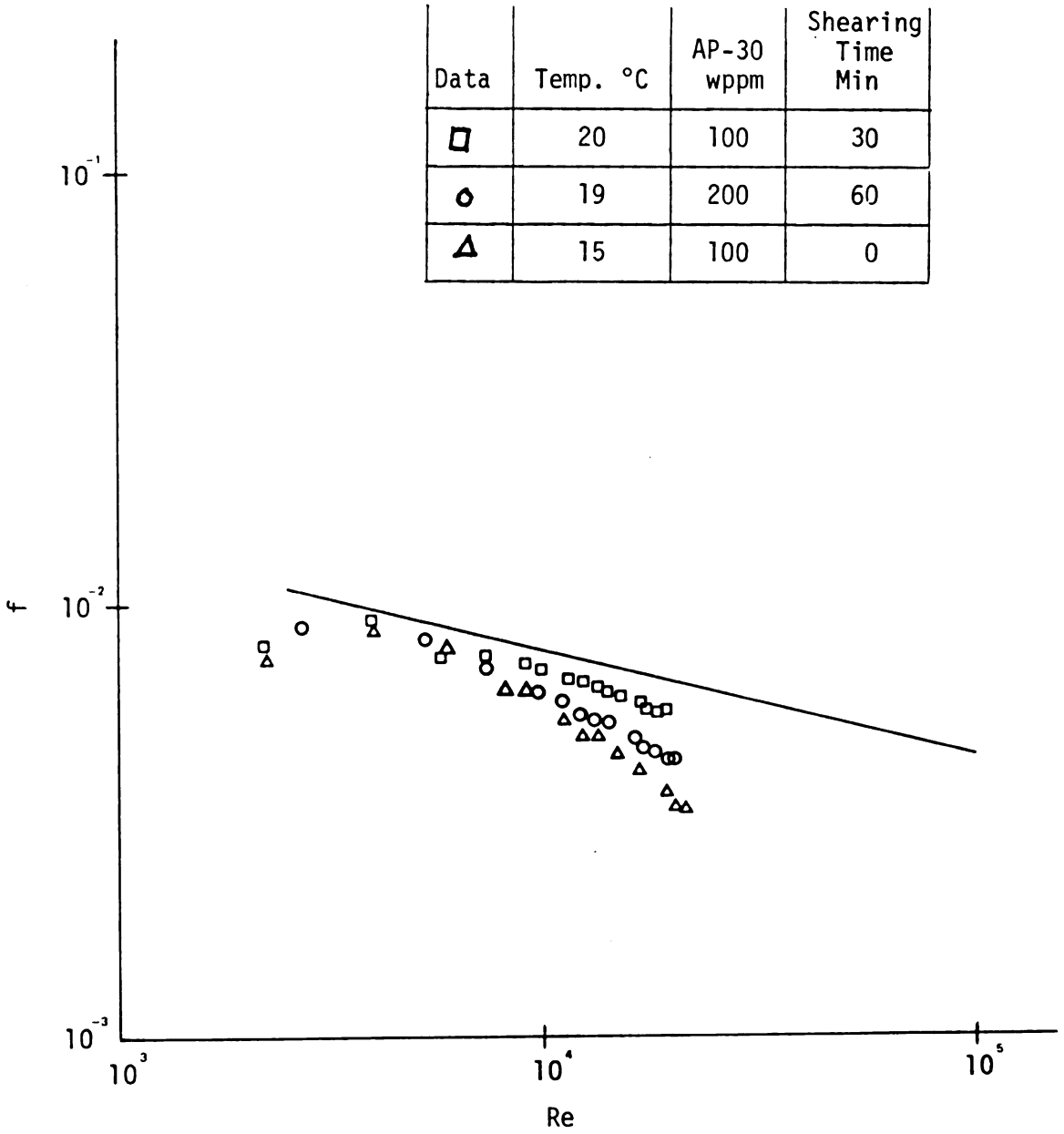

Figure A.5. The effect of shearing time on drag reduction.

Data	Temp °C	wppm AP-30	wppm Clay	Shear Time Min
▲	15	100	0	0
■	16	100	100	0

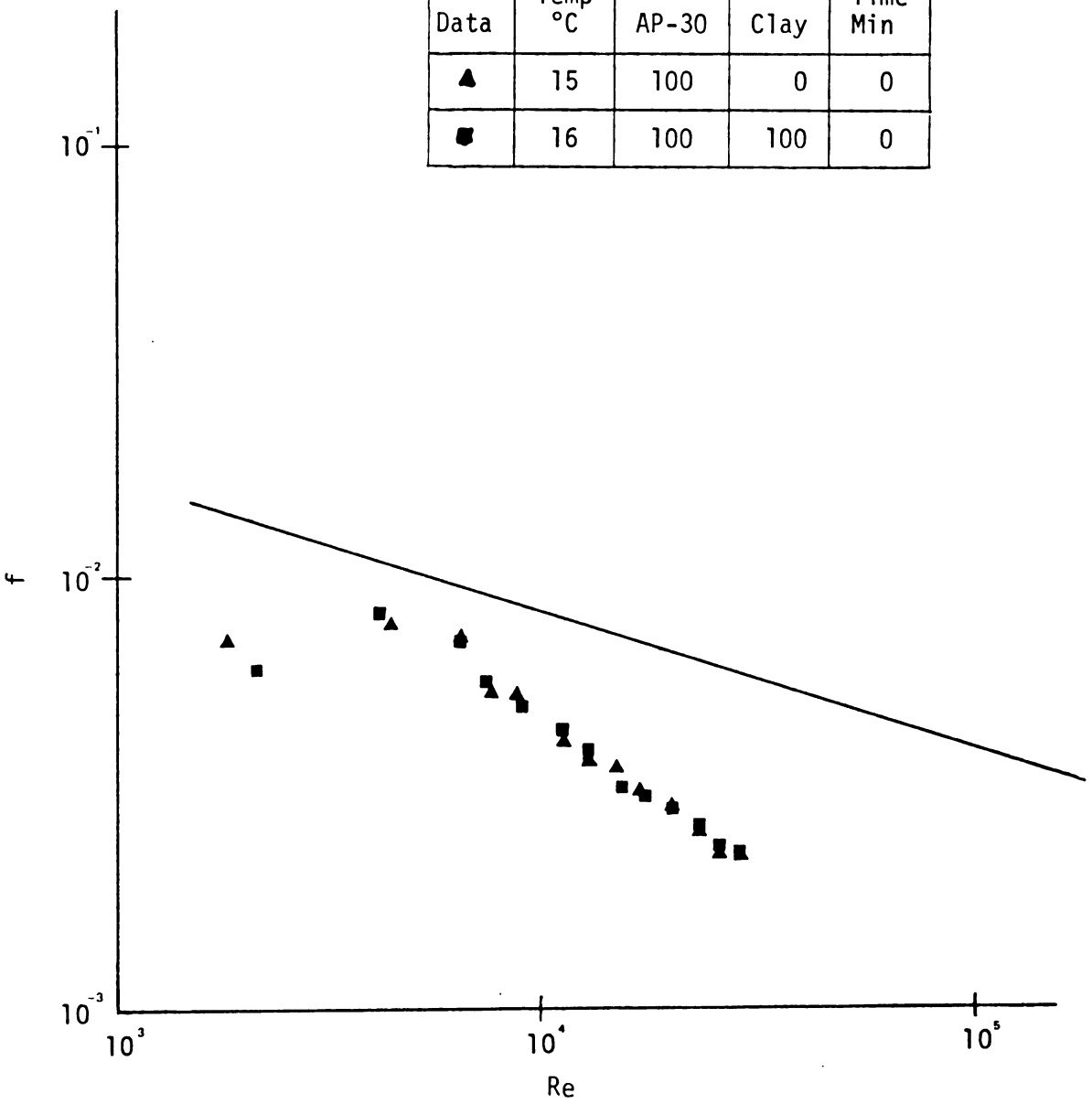

Figure A.6. The effect of clay concentration of drag reduction.

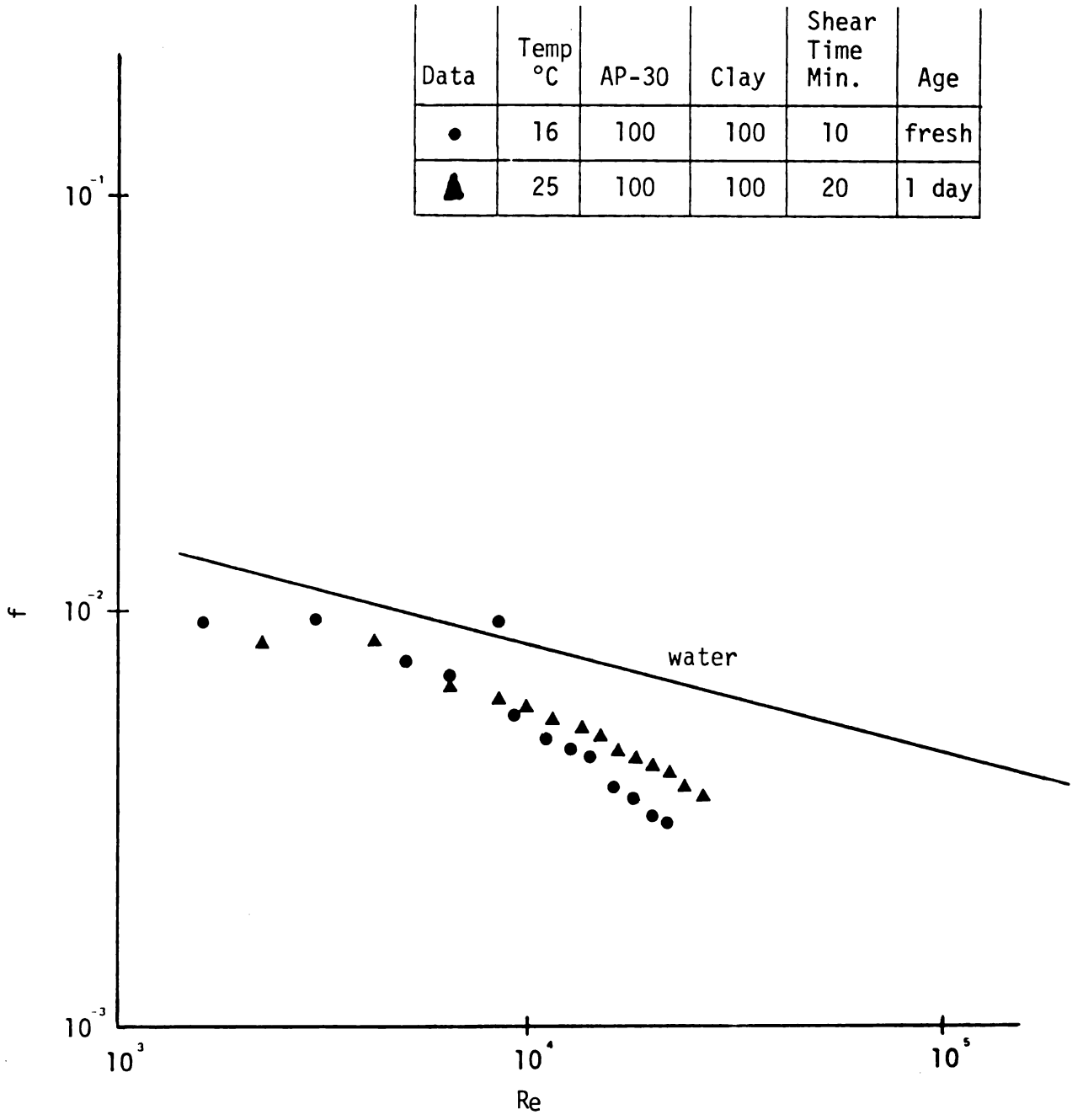

Figure A.7. The effect of polymer ageing on drag reduction.

polymer. The solution that sat overnight was sheared for 20 minutes. The only observable effect is a decrease in the drag reduction (an increase in the friction factor) which is more than likely due to the longer shearing time.

A.4 Summary

Drag reduction is definitely present in a solution containing Separan AP-30. The presence of clay, in small concentrations, and the mixing strategies have no significant effects on these properties. However, high concentrations of clay (2%) tend to dampen this effect. The drag reduction is transient in behavior. Its largest effect is noticeable when the polymer is first added to solution and quickly degrades as it is constantly recycled by the pumps. Complete degradation of the polymer is difficult. A residual amount of drag reduction remains after an hour of operation when further degradation has subsided.

APPENDIX B

EXPERIMENTAL DATA

TABLE B-1.--Experimental Data for Fully Developed Laminar Flow of a Fluid in a Circular Pipe. (D=0.146 in., L=89 in., ρ= 62.4 lb_m/ft^3, c = 100 wppm AP-30)

T (°C)	ΔH_c (in. CCl4)	W (lb_m/sec)	μ (cp)	Re	$fx10^3$
25.0	22.0	0.01385	1.075	2149	7.99
23.5	19.9	0.01288	1.046	1998	8.36
23.5	18.2	0.01209	1.019	1876	8.68
24.3	15.8	0.0184	0.986	1682	9.37
25.0	13.8	0.00959	0.974	1488	10.46
25.0	11.8	0.00821	0.973	1274	12.20
25.0	9.8	0.00680	0.975	1055	14.77
25.2	7.8	0.00537	0.983	833	18.85
24.9	6.05	0.00415	0.987	644	24.48
24.8	3.70	0.00253	0.990	393	40.28

TABLE B-2.--Experimental Data for Fully Developed Turbulent Flow of a Fluid in a Circular Pipe. (D=0.146 in., L=89, ρ=62.4 lb_m/ft^3, μ=1.024 cp, c=100 wppm AP-30, 100 wppm clay)

T (°C)	ΔH_m (in. Hg)	W (lb_m/sec)	Re x 10^{-4}	f x 10^3
25.0	56.25	0.1349	2.046	4.557
24.9	51.88	0.1271	1.928	4.734
24.4	47.88	0.1194	1.811	4.952
24.8	44.38	0.1131	1.715	5.114
24.8	39.94	0.1054	1.598	5.317
24.9	35.69	0.0982	1.489	5.457
24.9	31.69	0.0901	1.366	5.755
25.0	28.06	0.0833	1.263	5.937
24.9	23.25	0.0738	1.119	6.295
24.7	19.25	0.0651	0.987	6.697
24.5	15.50	0.0568	0.861	7.085
24.6	9.50	0.0438	0.664	7.301
24.8	5.50	0.0308	0.467	8.541
25.0	1.50	0.0162	0.246	8.431

TABLE B-3.--Experimental Data for Six 10mm Hydrocyclones (T=25°C, c=100 wppm AP-30, Po=Pu=0 psig)

P_F (psig)	Qo (GPM)	Qu (GPM)	Q_F (GPM)	$Re_F \times 10^{-4}$	Split Ratio (Qo/Qu)
98	3.54	2.36	5.90	3.28	1.500
90	3.41	2.24	5.65	3.14	1.522
80	3.35	2.09	5.44	3.03	1.603
70	3.23	1.96	5.19	2.89	1.648
60	3.09	1.77	4.86	2.70	1.746
50	2.86	1.59	4.45	2.48	1.799
40	2.72	1.36	4.08	2.27	2.000
35	2.56	1.33	3.89	2.17	1.925
30	2.36	1.28	3.64	2.03	1.844
25	2.10	1.32	3.42	1.90	1.591
20	1.71	1.45	3.16	1.76	1.179
10	1.09	1.35	2.44	1.36	0.809
5	0.88	1.23	2.11	1.17	0.715

TABLE B-4.--Performance Data for a 10mm Hydrocyclone (T=25°C, No AP-30, Po=Pu=0 psig).

P_F (psig)	Re_F x 10^{-4}	Overflow		Underflow		Feed		E
		Wo (lb_m/sec)	C_{clay} (wt.%)	W_u (lb_m/sec)	C_{clay} (wt.%)	W_F (lb_m/sec)	C_{clay} (wt.%)	
20	1.79	0.2070	0.148	0.2309	0.250	0.4379	0.204	0.2386
40	2.45	0.3659	0.150	0.2340	0.295	0.5999	0.206	0.2761
60	2.96	0.4195	0.145	0.3033	0.290	0.7228	-	0.2952
80	3.38	0.4573	0.141	0.3696	0.288	0.8269	0.2085	0.3222

REFERENCES

REFERENCES

Bradley, D., and Pulling, D. J., 1959. "Flow Patterns in the Hydraulic Cyclone and Their Interpretation in Terms of Performance," Trans. Inst. Chem. Engrs., 37, 34.

Bradley, D., 1965. The Hydrocyclone, Pergamon Press, Oxford.

Chiou, C. S., and Gordon, R. J., 1976. "Vortex Inhibition: Velocity Profile Measurements," AIChE J., 22, 947.

Dabir, B., Wallace, L. B., and Petty, C. A., 1980. I. Chem. E. Symposium Series No. 59, p. 5:9/1.

Dahlstrom, D. A., 1949. "Cyclone Operating Factors and Capacities on Coal and Refuse Slurries," Trans. Amer. Inst. Min. (Metall.) Engrs. 184, 331.

Fontein, F. L., Van Kooy, J. G. and Leniger, H. A., 1962. "The Influences of Some Variables upon Hydrocyclone Performance," British Chem. Eng., 1, 410.

Greenland, D. J., and Hayes, M. H. B., 1978. The Chemistry of Soil Constituents, Wiley, New York.

Haas, D. A., Nurmi, E. O., Whatley, M. E., and Engel, J. R., 1957. "Midget Hydrocyclones Remove Micron Particles," Chem. Eng. Progr. 53, 203.

Hillel, D., 1980. Fundamental of Soil Physics, Academic Press, New York.

Kelsall, D. F., 1952. "A Study of Solid Particles in a Hydraulic Cyclone," Trans. Instn. Chem. Engrs., 30, 81.

_____, 1953. "A Further Study of the Hydraulic Cyclone," Chem. Eng. Sci. 2, 254.

Matschke, D. E., and Dahlstrom, D. A., 1958. "Miniature Hydrocyclones Energy Requirements and Solid Elimination Efficiency Part I - Energy Requirements," Chem. Eng. Progr., 54, 60.

Michaels, A. S., and Morelos, O., 1955. "Polyelectrolyte Adsorption by Kaolinite," Ind. and Chem., 47, 1801.

Mitzmager, A., and Mizrahi, J., 1964. "Correlation of the Pressure Drop Through Small Cyclones Operating with Dilute Pulps of Various Liquids," Trans. Inst. Chem. Engrs., 42, 152.

Moder, J. J., and Dahlstrom, D. A., 1952. "Fine-Size, Close-Specific-Gravity Solid Separation with the Liquid-Solid Cyclone," Chem. Eng. Progr., 48, 74.

Pilgrim, R. F., and Ingraham, T. R., 1962. "Resolution of the Operating Variables of a Small Hydrocyclone," Can. J. Chem. Eng., Aug., p. 169.

Rietema, K., 1961. "Performance and Design of Hydrocyclone I-IV, Chem. Eng. Sci., 15, 298.

Schmidt, R. A., and Hill, G. R., 1976. "Coal: Energy Keystone," Annual Review of Energy, 1, 37.

Van Ebbenhorst Tengbergen, H. J., 1961. "The Separation of Liquids from Gases by Cyclones," in Cyclones in Industry, K. Rietema and C. G. Verver, Ed., Elsevier, Amsterdam.

Virk, P. S., 1975. "Drag Reduction Fundamentals," AIChE, 21, 625.

Wallace, L. B., 1980. "The Effect of Polyacrylimide on the Performance of a Hydrocyclone," M. S. Thesis, Michigan State University.

Weast, R. C., Ed. 1981. Handbook of Chemistry and Physics, 62nd edition. CRC, Cleveland.